Bulletin of Earthquake Engineering
https://doi.org/10.1007/s10518-023-01636-8

ORIGINAL ARTICLE

Typological fragility analysis of masonry buildings in Emilia Romagna region (Italy)

Francesca Ferretti[1] · **Elena Simoni**[1] · **Nicola Buratti**[1] · **Claudio Mazzotti**[1]

Received: 23 August 2022 / Accepted: 28 January 2023

Abstract
UnReinforced Masonry (URM) buildings constitute the majority of the Italian building stock and represent one of the most vulnerable construction typologies, as emerged during the seismic events occurred in the last decades. The objective of the present work is the proposal of a methodology for the seismic vulnerability and fragility assessment of different typologies of URM buildings. Through the statistical analysis of post-earthquake damage survey forms and of census data, the most prevalent structural typologies were identified in the Emilia Romagna region (Italy), leading to the definition of two reference masonry buildings, built at the beginning of the XX century and representative of the building stock of the study area. These buildings were modeled according to the equivalent frame method and their seismic performance was studied by means of nonlinear static analyses, considering uncertainties on the mechanical properties of masonry, on the intensity of the seismic action and on the displacement demand calculation method. Through the definition of Response Surfaces, analytical fragility curves relative to the investigated structural typologies were determined for the different damage states.

Keywords Masonry building · Seismic behavior · Nonlinear static analyses · Fragility assessment

✉ Francesca Ferretti
francesca.ferretti10@unibo.it

Elena Simoni
elena.simoni@outlook.com

Nicola Buratti
nicola.buratti@unibo.it

Claudio Mazzotti
claudio.mazzotti@unibo.it

[1] Department of Civil, Chemical, Environmental and Materials Engineering, University of Bologna, Viale Risorgimento 2, 40136 Bologna, Italy

Published online: 22 February 2023

1 Introduction

The seismic vulnerability of existing UnReinforced Masonry (URM) buildings is a relevant issue for many European countries, because of the age of their building stock, built without a proper seismic approach and often suffering materials deterioration (Ceroni et al. 2012; Parisi and Augenti 2013). At the same time, the safety assessment of historical constructions is complicated by their geometrical complexity, the variability of material properties, the poor knowledge on past events which might have affected the current condition of the constructions and the lack of specific design codes (Lourenço et al. 2011; Indirli et al. 2013; Penna et al. 2014b). Over time, there has been a progressive evolution of the construction techniques, resulting in a great variety of structural typologies, in terms of configuration in plan and in elevation, of mechanical properties of the masonry, of the type of horizontal structural elements, i.e., slabs and roofs, and of their connections to the vertical masonry walls. As a consequence, the study of the seismic behavior of masonry buildings is associated to a large number of uncertainties (Sousa et al. 2016). Therefore, probabilistic methods are recommended to carry out quantitative assessments of structural safety (Parisi and Augenti 2012). In this framework, the seismic structural safety of existing buildings is often expressed in the form of fragility curves (Buratti et al. 2010), which define the probability of exceeding specific damage levels as a function of the intensity of the seismic ground-motion.

Seismic fragility curves can be obtained by means of numerical simulations (Silva et al. 2014; Rota et al. 2014; Simões et al. 2015; Milosevic et al. 2020; Battaglia et al. 2021), statistical analysis of observational damage data (Rota et al. 2008; Ioannou et al. 2021) or engineering judgment (Jaiswal et al. 2011). To calibrate fragility curves through numerical simulations it is necessary to develop nonlinear models that describe the behavior of structures subject to ground-motions, reproducing their failure modes. Given the large number of uncertainties involved in the problem, rigorous probabilistic models are often unpractical and approximate approaches are often preferred (Milani and Benasciutti 2010; Bracchi et al. 2015).

The development of detailed vulnerability models at a territorial scale requires the identification of different building classes or typologies and the definition of the factors mostly affecting their structural response. Indeed, buildings with similar architectural and structural features, located in similar geotechnical conditions, are expected to have similar performances in the event of an earthquake.

The objective of the present paper is the proposal of a procedure for the evaluation of the seismic fragility of different classes of URM buildings, through the definition of two case studies, representative of a relevant part of the building stock of the Emilia Romagna region. Their structural capacity was defined by applying two different displacement demand calculation methods on the capacity curves, obtained from nonlinear static analyses (pushover). The variability of the seismic action was taken into account by adopting response spectra of recorded accelerograms suitable for the displacement demand estimate. The uncertainties related to the structural behavior of the case studies were considered by assuming the mechanical properties of masonry as random variables and by adopting a Response Surface (RS) model (Faravelli 1989; Rajashekhar and Ellingwood 1993; Franchin et al. 2003): a statistical model which allows to define the dependency of the structural capacity on a set of factors, through simplified analytical relationships (Buratti et al. 2010). Fragility curves were then obtained with reference to

four damage states, accounting for uncertainties related to the mechanical properties of masonry, to the seismic action and to the displacement demand calculation method.

2 Identification of the building typologies

In this work, building types were defined by considering information gathered from two databases including information about the residential URM buildings of the Emilia Romagna region: (i) the 2011 Italian census, by the Italian National Institute of Statistics (ISTAT) and (ii) the post-earthquake damage survey, collected by the Italian Department of Civil Protection after the 2012 Emilia earthquake through the AeDES (Accessibility and Damage detection in the post-Seismic Emergency) form (Baggio et al. 2002). Both databases contain information, for each building, about the adopted structural technology (concrete, masonry, etc.…), the construction period, and the number of floors. In addition, the AeDES forms contain further data about the structural components as well as the level and the extent of damage. In more detail, vertical and horizontal structural elements are classified, the quality of materials is visually assessed and the presence of structural features that might affect the seismic behavior (such as steel ties, bond beams or ring beams, irregularities either in plan or in elevation) are reported. The damage states are classified based on a five levels scale: no damage (DS0), slight damage (DS1), medium or heavy damage (DS2–DS3), severe or very heavy damage, even leading to collapse (DS4–DS5).

A statistical analysis of these combined sets of data can lead not only to the identification of the prevalent structural types in the Emilia Romagna region, but also to the definition of the structural characteristics associated with the most severe damage. To obtain a more uniform dataset, the analysis of the census data was limited to the municipalities located in the area stroke by the 2012 Emilia earthquakes, belonging to the provinces of Bologna, Modena and Ferrara. A total of 110,655 URMbuildings was obtained from the census data, while 29,322 buildings, representing a data subset of the census data, were considered by the AeDES forms, which were filled upon request after the seismic events. The graphs presented in Figs. 1 and 2 show the distribution of the buildings according to the construction period and the number of floors for the two data sources. It can be noticed that the biggest amount of buildings were built before 1919 and that they were mainly characterized by the presence of two or three floors above ground.

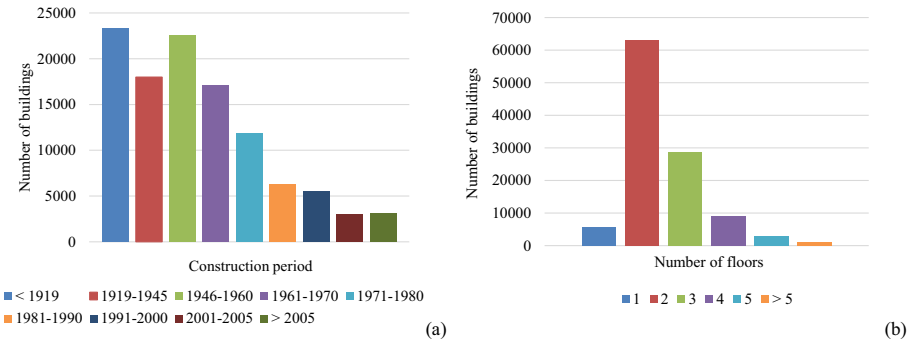

Fig. 1 Distribution of the buildings (ISTAT) according to: **a** construction period, **b** number of floors

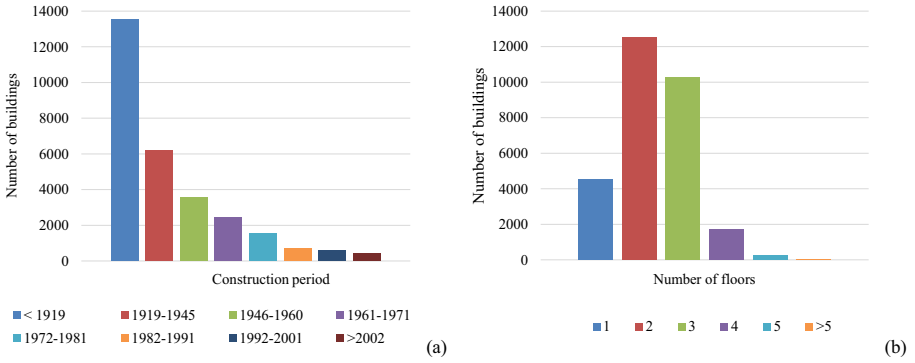

Fig. 2 Distribution of the buildings (AeDES form) according to: **a** construction period, **b** number of floors

Considering the data collected from the post-earthquake surveys (AeDES), it was possible to investigate the damage distribution for the different construction periods: its graphical representation (Fig. 3a) shows that the newer the buildings, the lighter the damage produced. Moreover, it can be observed that the highest percentages of buildings with the most severe damage (either DS4 or DS5) referred to the construction period prior to 1919. The most frequent case, among the presented data, was represented by buildings built before 1919, with either 2 or 3 floors above ground and damage state DS4. For this combination of parameters, the type of vertical and horizontal structural elements was further investigated (Fig. 3b, c). The number of buildings having a regular or irregular masonry bond pattern is reported in Fig. 3b, while the distribution of the different types of horizontal structural elements is shown in Fig. 3c. The majority of the buildings of the considered sub-category were characterized by a regular configuration in plan (69.8%) and by the presence of light-weight thrusting (40.3%) or light-weight non-thrusting (39.3%) roofing elements.

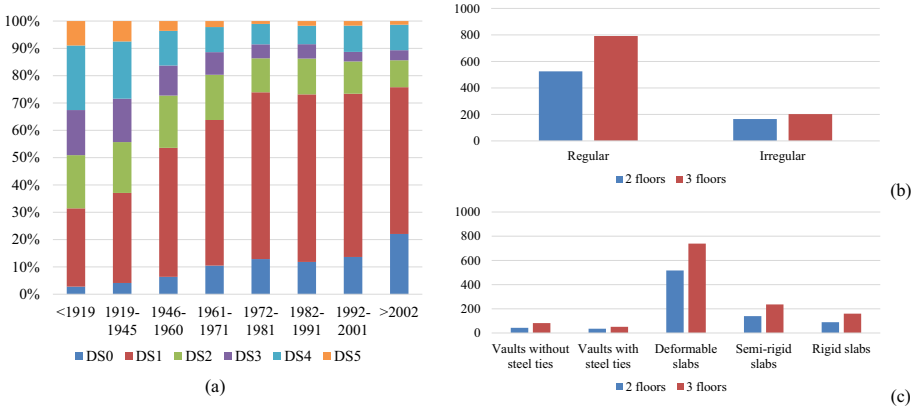

Fig. 3 **a** Damage state distribution according to the construction period, **b** masonry bond pattern distribution (< 1919, DS4), **c** horizontal structural element distribution (< 1919, DS4)

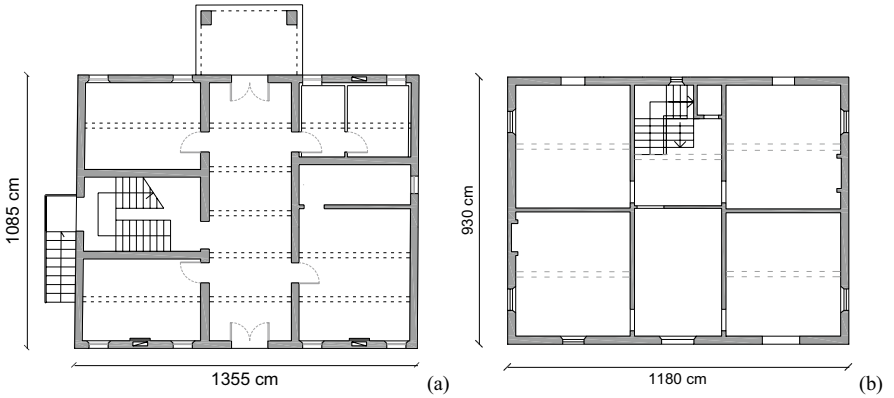

Fig. 4 Plan view of the modelled buildings: **a** BT1, **b** BT2

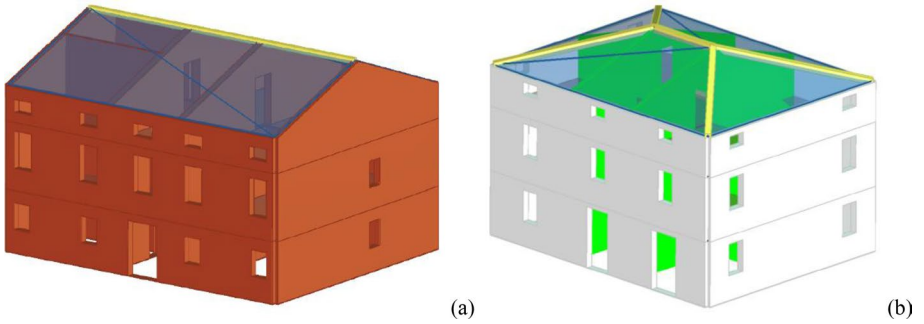

Fig. 5 3D model of the buildings: **a** BT1, **b** BT2

Based on the statistical analysis of the databases here presented, two representative building types were considered in this research for the fragility assessment. They are described in Section 3.

3 Case study buildings

Two existing buildings, having the characteristics identified by means of the statistical analysis presented in Sect. 2, were selected in this research for the determination of analytical fragility curves. These real buildings were built before 1919 and they are representative of the portion of the Emilia-Romagna building stock dating back to the beginning of the XX century. Their plan view is similar and very regular, as shown in Fig. 4, and in elevation they both feature 2 floors and an attic. The first building (BT1) is a brick masonry building with a regular bond pattern, while the second building (BT2) has stone masonry external walls and brick masonry internal walls. Both buildings have deformable timber slabs and roofing elements.

The two buildings were modelled with the software 3Muri (Fig. 5), based on the equivalent frame modelling approach, to perform nonlinear static (pushover) analyses

(Lagomarsino et al. 2013; Penna et al. 2014a). All the geometric data needed in the modelling phase and the data needed for the load analysis of the slabs and the roof were directly derived from surveys on the buildings. With the aim of investigating the seismic behavior of different building typologies, three distinct models were considered based on the characteristics of the selected buildings:

- BT1_BM: the first building was modeled by considering all the walls as constituted by clay brick masonry and by adopting a shear failure criterion according to the Mann and Müller's theory, which is appropriate for masonries characterized by a regular bond pattern (Mann and Muller 1980);
- BT2_SM: the second building was modeled by considering all the walls as constituted by stone masonry and by adopting the Turnšek-Čačovič's shear failure criterion (Turnsek and Cacovic 1971);
- BT2_SM-BM: the second building was modeled by considering the external walls constituted by stone masonry and the internal walls constituted by clay brick masonry. The Turnšek-Čačovič's shear failure criterion (Turnsek and Cacovic 1971) was adopted for all the walls for sake of consistency.

The mechanical properties of masonry, in terms of compressive strength (f_m), shear strength (τ_0 or f_{v0}), Young's modulus (E) and shear modulus (G), were assigned to the masonry piers and spandrels according to the recommended ranges provided by the Italian Building Code (Ministero delle Infrastrutture e dei Trasporti 2018, 2019) for existing buildings, reported in Table 1. In more detail, concerning the shear strength, the parameter τ_0 controls the diagonal cracking failure mode according to the Turnšek-Čačovič's criterion (1971), while the parameter f_{v0} controls the stair-stepped diagonal cracking according to the Mann-Müller's criterion (Mann and Muller 1980). Confidence factors, to be used when dealing with existing buildings to reduce the mean mechanical properties of Table 1 according to the knowledge level, and partial safety factors were considered equal to 1.

To account for uncertainties in the structural behavior, nonlinear static analyses were performed by considering several permutations of the mechanical properties of the masonry walls. The permutations were defined by combining the minimum and the maximum values of the parameters f_m, τ_0 or f_{v0}, E and G (Table 1), according to the Design of Experiments theory (Box and Draper 1987; Khuri and Cornell 1997) with a two-level factorial design (Box and Wilson 1951). A total of 2^n permutations were obtained for each model, being n the number of independent variables, plus an additional permutation in which all the parameters were set to their average value. The Young's and the shear modulus were considered dependent on each other; therefore, their ratios did not change in the

Table 1 Mechanical properties of the masonry typologies (Ministero delle Infrastrutture e dei Trasporti 2019)

Masonry typology		f_m (MPa)	τ_0 (MPa)	f_{v0} (MPa)	E (MPa)	G (MPa)	w (kN/m^3)
Clay brick with lime-based mortar	Min	2.60	0.05	0.13	1200	400	18
	Avg	3.45	0.09	0.20	1500	500	
	Max	4.30	0.13	0.27	1800	600	
Stone masonry with regular bond pattern	Min	2.60	0.056	–	1500	500	21
	Avg	3.20	0.065	–	1740	580	
	Max	3.80	0.074	–	1980	660	

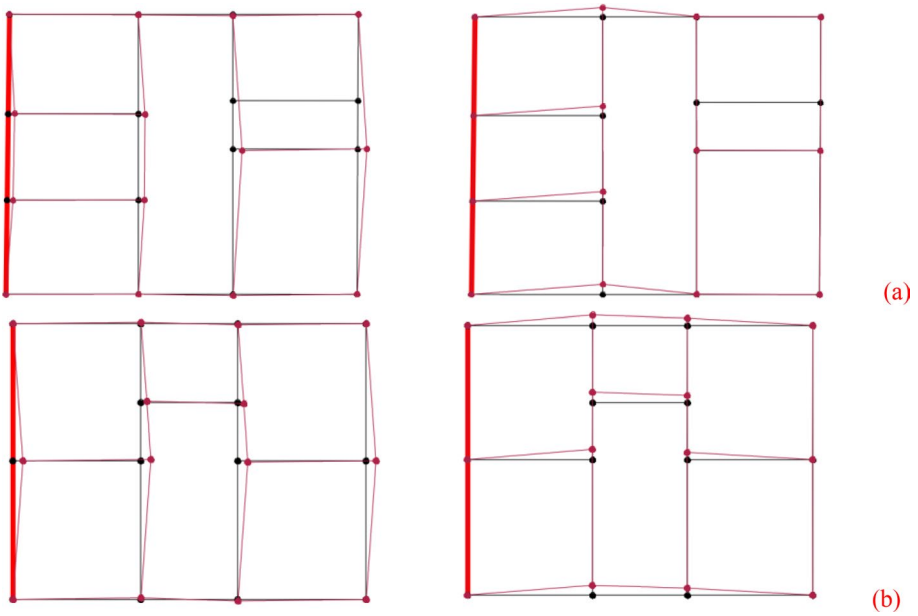

Fig. 6 Mode shapes in *X* and *Y* directions for the buildings: **a** BT1_BM, **b** BT2_SM and BT2_SM-BM

Table 2 Fundamental periods of first mode shapes of the investigated buildings

Building	T (s)	
	X direction	*Y* direction
BT1_BM	0.13	0.16
BT2_SM	0.23	0.20
BT2_SM-BM	0.24	0.21

permutations. For the models BT1_BM and BT1_SM, constituted by a unique masonry typology, 9 permutations were obtained, while 65 permutations were obtained for the model BT2_SM-BM, given the presence of two distinct masonry typologies.

As an example of the dynamic characteristics of the investigated buildings, Fig. 6 shows the first modes of vibration in the *X* and *Y* directions for the permutation with the average values of mechanical parameters, while the fundamental periods are reported in Table 2.

4 Capacity curves

4.1 Nonlinear static analysis

For each model, different nonlinear static (pushover) analyses were performed by considering two different distributions of lateral forces applied along the two main horizontal directions ($\pm X$ and $\pm Y$) and their corresponding accidental eccentricities, i.e., -5%, 0%, and $+5\%$ of the building width in each direction. According to the Italian Building Code (Ministero delle Infrastrutture e dei Trasporti 2018), the first lateral load distribution is

proportional to the shape of the fundamental mode of vibration in each direction, while the second is uniform along the height. These distributions will be indicated in the following as *modal* and *uniform*, respectively. Combining the 2 different lateral load distributions, the 4 loading directions and the 3 values of accidental eccentricity, a total of 24 capacity curves were obtained for each permutation of the material properties. These curves were then converted into capacity curves for equivalent Single-Degree-Of-Freedom (SDOF) systems whose base shear (F_b*) and displacement (d_c*) were computed from the capacity curves from the Multi-Degree-Of-Freedom (MDOF) model (F_b, d_c), as:

$$\begin{aligned} F_b^* &= \frac{F_b}{\Gamma} \\ d_c^* &= \frac{d_c}{\Gamma} \end{aligned}, \tag{1}$$

where Γ is the modal participation factor for the force distribution considered (Fajfar 1999, 2000). The curves for the equivalent SDOF systems were then approximated by means of elastic–plastic curves. The bilinearization technique was based on energy equivalence principles, while the ultimate displacement was defined, according to the indications of the Italian Building Code for the collapse limit state (Ministero delle Infrastrutture e dei Trasporti 2018, 2019), as the minimum between the displacement associated with 20% reduction of the base shear after the maximum of the capacity curve and the displacement corresponding to the collapse of the masonry piers belonging to any wall considered relevant for the safety of the construction on any floor of the building.

In Fig. 7 and Fig. 8, a selection of the capacity curves (for the MDOF model) obtained from the models BT1_BM and BT1_SM is reported, considering the permutations in terms of shear strength, for which the other mechanical parameters were equal to their maximum value. Directions $+X$ and $+Y$ are considered separately. As expected, by increasing the shear strength value, the shear capacity increased. For the model BT2_SM-BM, three sets of capacity curves are presented in Fig. 9, considering the permutations in terms of shear strength for both the stone masonry and the brick masonry. In the selected permutations, all the other mechanical parameters were set at their maximum value. Variations of both shear strength values (i.e., for brick and stone masonry) led to an increased capacity, in terms of maximum base shear and maximum displacement. Results of the pushover analyses showed, in general, that the masonry piers were failing mainly for shear (see Fig. 10 in

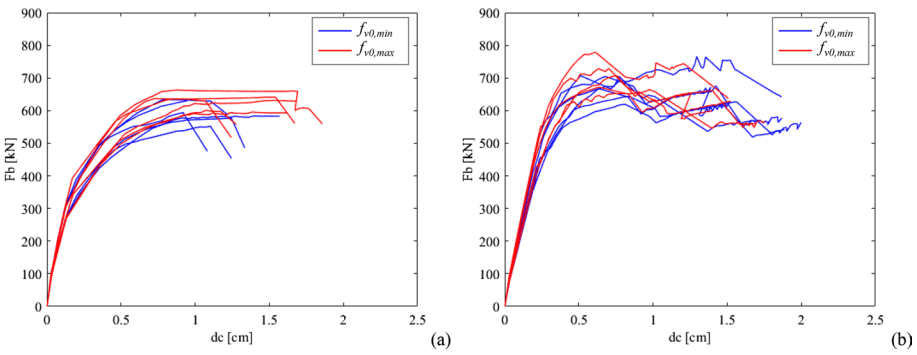

Fig. 7 Capacity curves for the model BT1_BM with permutations in terms of shear strength f_{v0}: **a** $+X$ direction, **b** $+Y$ direction

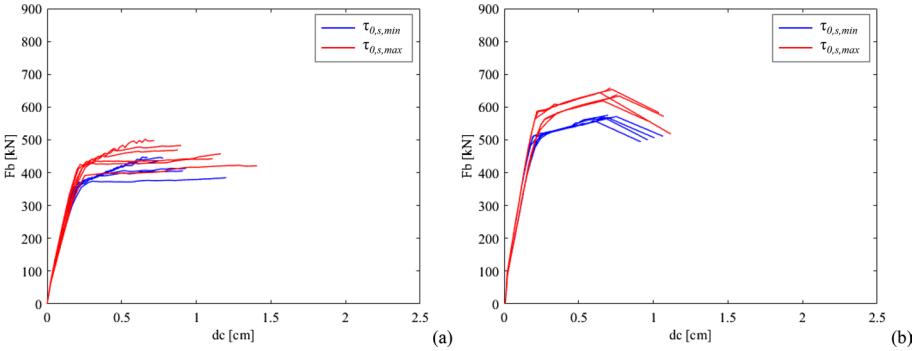

Fig. 8 Capacity curves for the model BT2_SM with permutations in terms of stone masonry shear strength $\tau_{0,s}$: **a** + *X* direction, **b** + *Y* direction

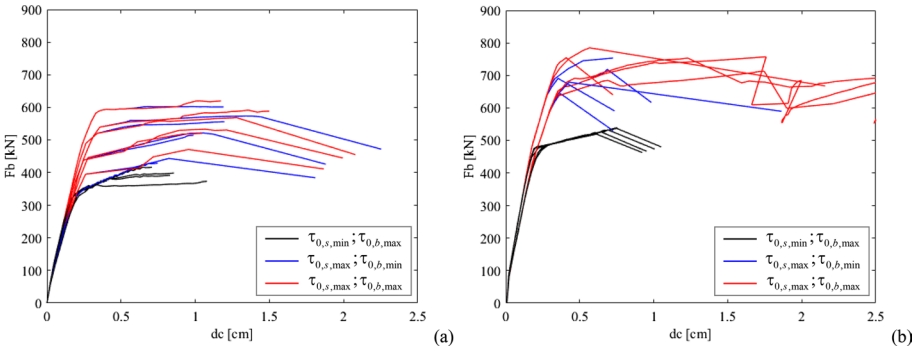

Fig. 9 Capacity curves for the model BT2_SM-BM with permutations in terms of shear strength $\tau_{0,s}$ and $\tau_{0,b}$: **a** + *X* direction, **b** + *Y* direction

which representative failure modes are reported) and this was coherent with the effect that a variation in the shear strength had on the capacity curves.

4.2 Damage state definition

As evidenced in a recent work (Cattari and Angiolilli 2022), the debate about the definition of damage levels for masonry buildings is still open. Several methods exist, some of which based on a multiscale approach, some others based on the definition of specific thresholds for a unique parameter, e.g. roof drift, interstory drift ratio, etc. (Lagomarsino and Cattari 2015). Previous works, starting from the proposal by Calvi (1999), defined the damage states in terms of specific displacement values on the pushover curves (Cattari et al. 2004, 2014; Lagomarsino and Giovinazzi 2006). Given the regularity and simplicity of the investigated buildings, this method was here adopted, instead of the multiscale approach, which is more suitable when dealing with large and complex constructions (Lagomarsino and Cattari 2015).

According to the adopted damage scale, an expected structural performance is assigned to each damage state, as described in Table 3. The reported damage states were associated

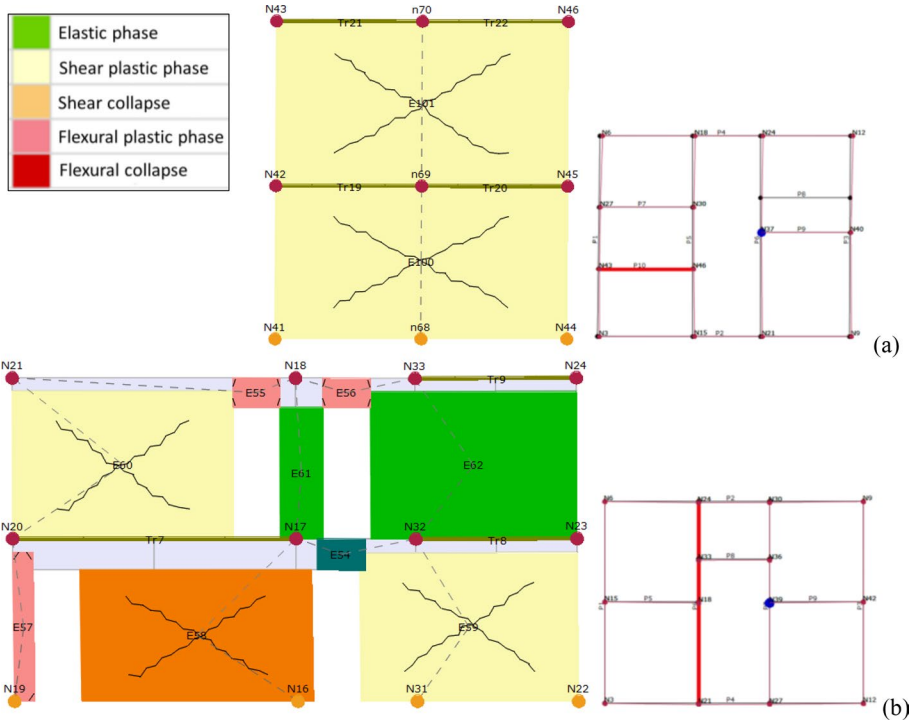

Fig. 10 Representative failure modes of the masonry walls for: **a** model BT1_BM, **b** model BT2_SM

to different points on the capacity curves as a function of either the yielding displacement d_y or the ultimate displacement d_u according to Eq. (2):

$$\begin{aligned} S_{d,D1} &= 0.7d_y \\ S_{d,D2} &= 1.5d_y \\ S_{d,D3} &= 0.5(d_y + d_u) \\ S_{d,D4} &= d_u \end{aligned} \tag{2}$$

Fig. 11 shows an example of application of the criteria from Eq. (2), where the coloured points represent the different displacement values associated with each damage level.

5 Seismic displacement demand

Given a capacity curve and a seismic action in the form of an elastic response spectrum, it is possible to estimate the maximum displacement that a structure will attain during a seismic ground-motion, also referred to as performance point. According to both the Italian Building code (Ministero delle Infrastrutture e dei Trasporti 2018) and the Eurocode 8 (CEN 2004), two approaches can be adopted to evaluate the seismic displacement demand. The first accepted methodology is known as N2 Method, and it is based on empirical R-μ-T relationships (Fajfar and Fischinger 1988; Vidic et al. 1994; Fajfar 1999, 2000). The

Table 3 Definitions of damage limit states (Calvi 1999)

Damage state	Structural damage	Non-structural damage	Description
D_0	None	None	Undamaged building
D_1	None	Minor	The expected response can be assumed linear elastic as yielding is not reached in any critical section
D_2	Minor	Moderate	The building can still be occupied after the earthquake without needing of provisions or interventions
D_3	Significant	Extensive	The building must be repaired before use. Repair and strengthening can still be done at this damage state
D_4	Complete	Complete	The building collapses and cannot be repaired either from a practical or economical point of view

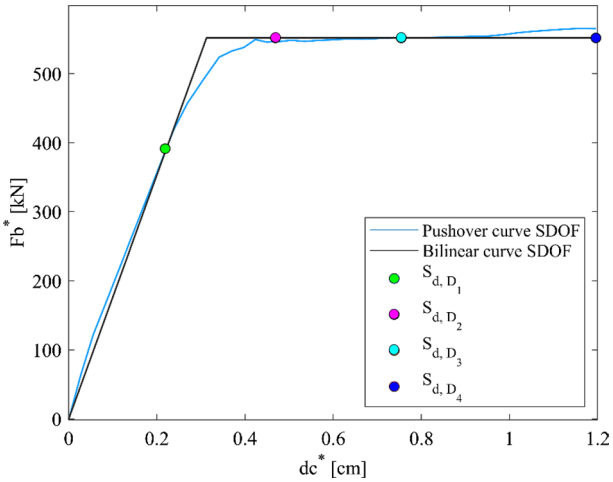

Fig. 11 Identification of the damage states on the SDOF bilinear curve

second procedure is the Capacity Spectrum Method, defined in ATC-40 (Applied Technology Council 1996) and included in FEMA-247 (FEMA 1999). It is based on the definition of an equivalent viscous damping ratio related to the dissipative capacity of the structure under consideration. In the present research, the uncertainty related to the choice of the displacement demand calculation method was considered. Therefore, the two different approaches were employed in the seismic demand computation.

5.1 N2 method

The first method adopted for computing the displacement demand was the N2 Method as modified by Guerrini et al. (2017). These authors derived R-μ-T relationships for short-period URM buildings by considering two MDOF systems that were representative of two limit-configurations: flexural dominated structures with slender piers and shear dominated structures characterised by squat piers. From both models, equivalent SDOF systems were calibrated so that the hysteretic demand would coincide between the associated MDOF and SDOF systems. The dissipative hysteretic capacity per cycle was quantified by means of the Jacobsen's equivalent damping ratio $\xi_{hyst.}$ (Jacobsen 1930). The SDOF response was then evaluated through several hysteretic models, featuring different slopes of the initial acceleration *vs* displacement curve, different elastic periods T_0, masses m and viscous damping coefficient values (ξ_{vd}). Capacity curves for each model were transformed into equivalent elastic–plastic relationships through equivalence of the underlying areas of the base shear *vs* displacement diagram, starting from the origin of the axes up to the collapse point. The collapse displacement was identified as described in Section 4.1. The secant stiffness was evaluated in correspondence with the 70% of the maximum base shear, while the corresponding elastic period T^* was computed as:

$$T^* = 2\pi\sqrt{\frac{m}{k}}, \tag{3}$$

where m and k are the mass and the stiffness of the SDOF system, respectively.

The force reduction factor R was instead obtained from the elasto-plastic curve by following the relationship:

$$R = \frac{d_e}{d_y} = \frac{a_e}{a_y} = \frac{F_e}{F_y}, \tag{4}$$

where $d_e = a_e \cdot (T/2\pi)^2$ is the elastic displacement demand, $a_e = S_e(T^*)$ is the pseudo-spectral acceleration associated with the elastic period T^* and a damping ratio $\xi = 5\%$, and $F_e = m \cdot a_e$ is the corresponding elastic force. Then, $d_y = a_y \cdot (T/2\pi)^2$ is the displacement demand at yielding, a_y is the pseudo-spectral acceleration at yielding and $F_y = m \cdot a_y$ is the associated yielding force. Guerrini et al. studied the response of a variety of SDOF systems by means of nonlinear dynamic analyses, considering many combinations of elastic periods, pseudo-spectral acceleration or force-reduction factor, and they obtained the formulation for the displacement demand. In particular, for force reduction factor $R \geq 1$, Guerrini et al. proposed the following equation for evaluating the inelastic displacement d_{max}:

$$d_{\max} = \frac{d_e}{R}\left[\frac{(R-1)^c}{\left(\frac{T}{T_{hyst}} + a_{hyst}\right)\left(\frac{T}{T_c}\right)^b} + R\right], \tag{5}$$

where T_{hyst}, a_{hyst}, b and c are parameters calibrated by Guerrini et al. (Guerrini et al. 2017) by analysing the dynamic response of the first SDOF systems defined. If $R < 1$, instead, $d_{max} = d_e$.Capacity Spectrum Method.

The Capacity Spectrum Method (CSM), first proposed by Freeman (Freeman 1994, 2004), estimates the displacement demand through elastic spectra scaled by viscous damping coefficients associated to the hysteretic dissipation. The comparison between demand and capacity, in this method, was implemented in the Acceleration-Displacement Response Spectra (ADRS) plane. To express the capacity curve in terms of acceleration *vs* displacement, the relationships presented in Eq. (6) were used:

$$\begin{aligned} a_{ADRS} &= \frac{F_b^*}{M\alpha_1} \\ d_{ADRS} &= d_c^* \varphi_1 \end{aligned}, \tag{6}$$

where d_c^* and F_b^* are the displacement and the base shear of the SDOF capacity curve, M is the total mass of the building, α_1 is the effective modal mass ratio for the force distribution considered, while φ_1 is the amplitude of the force distribution at the control point. After defining an initial tentative value of the performance displacement d_{pi}, the associated dissipated energy was obtained and the equivalent viscous damping ξ_{eq} was computed as well according to the expression:

$$\xi_{eq} = k\frac{2}{\pi}\frac{\left(F_y^{*(0)} d_{\max}^{*(0)} - F_{\max}^{*(0)} d_y^{*(0)}\right)}{F_{\max}^{*(0)} d_{\max}^{*(0)}} + 0.05, \tag{7}$$

where $k = 0.33$ was taken from ATC-40 (Applied Technology Council 1996) with reference to poor existing buildings and short shaking duration (Structural Behaviour Type C). This parameter was used to calculate the reduced elastic spectrum. Then, the intersection between the scaled elastic spectrum and the capacity curve represented the performance point, d_{pi+1}. If this point was close to the initial guess d_{pi}, then d_{pi+1} was taken as the

displacement demand (d_{max}), otherwise the iterative process continued until convergence of the solution and d_{pi+1} was considered as a new tentative displacement.

6 Definition of seismic actions

In the present work, seismic actions were represented through the response spectra of recorded accelerograms, which were selected based on spectral compatibility with elastic target response spectra with the shape adopted by the Italian Building Code. To find the target spectra for the accelerogram selection, the capacity curves obtained for the models with a unique masonry typology (BT1_BM and BT2_SM) were considered, selecting the permutation in which all the mechanical parameters were set to their average value (Table 1). By means of the N2 method, they were used to determine the return period of the code spectra that led to displacement demands equal, on average, to the displacement capacities associated to each of the four damage states under consideration (see Section 4.2). The elastic spectra in Fig. 12 represent the target for the accelerogram selection procedure, with values of the return period reported in the legend. It was checked that the target spectra obtained for the model BT2_SM could be used as target spectra also for the model BT2_SM-BM. Clearly the target spectra are characterized by return periods much higher than the ones which are usually considered in design applications, because, on one hand, the damage states considered are more severe that those conventionally adopted by building codes and, on the other hand, mean values of material strengths are used. The procedure adopted allowed to identify response spectra that are consistent with the uniform hazard spectra while limiting the need for scaling.

Spectral compatibility was searched for a range of periods including the elastic and secant periods of vibration of the studied structures, specifically from 0.1 to 0.7 s. Recorded accelerogram response spectra were selected from the PEER Ground motion database (Pacific Earthquake Engineering Research Center), precisely referring to the NGAWest2 project. To account for variability in the seismic action, 40 accelerograms were selected for each damage state and for each model. The following criteria were introduced in the selection: (i) restrictions in terms of soil category were considered, selecting a range of $V_{S,30}$ values that allowed to include only recordings on soil class B and C (i.e., 180 m/s $\leq V_{S,30} \leq$ 800 m/s), as defined by the Italian Building Code; (ii)

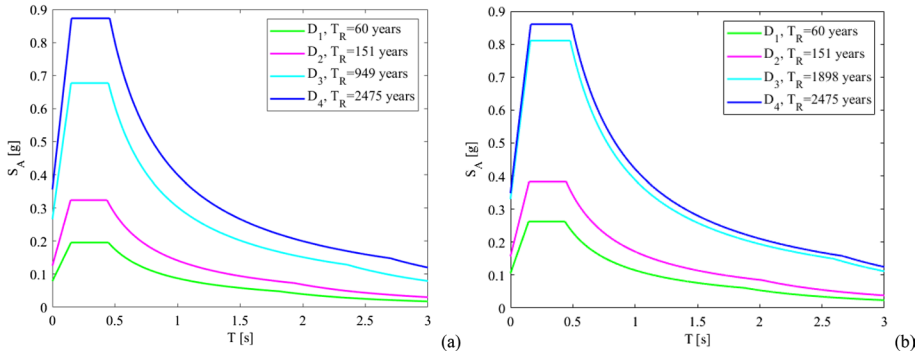

Fig. 12 Target elastic spectra for four damage limit states: **a** BT1_BM, **b** BT2_SM and BT2_SM-BM

impulsive records were excluded; (iii) a maximum of 4 records per earthquake was used. After this preliminary selection, the remaining accelerograms were sorted according to the value of their average root-mean squared deviation (RMSD) from the target spectrum and the 40 accelerograms with the lowest RSMD value were considered. The accelerograms selection was carried out by using the PSARotD50, as defined by Boore et al. (2006), namely the 50th percentile of the values obtained from the rotation of the acceleration horizontal components from 0° to 180°. As an example, in Fig. 13 the accelerograms selection for the model BT1_BM is reported for each damage state: the grey and red curves represent the spectra from the selected accelerograms and the average ones, respectively, while the black curves represent the target spectra (Fig. 12a). The complete list of the selected accelerograms for all the models and damage states is reported in the Appendix: for each registration, the earthquake name and year are reported together with the recording station name, the moment magnitude, the Joyner-Booree source-to-site distance and the value of $V_{S,30}$.

The pseudo-acceleration spectra for two orthogonal horizontal directions were used in the analysis. Recordings, however, came from different sources and events and thus the horizontal components did not always correspond to the N-S and E-W directions, which was the most common notation. To avoid confusion, in the following paragraphs, the components will be referred to as H_1 and H_2 as to identify two generic perpendicular horizontal components. Due to the unknown orientation of the typological buildings with respect to the two acceleration components of the seismic

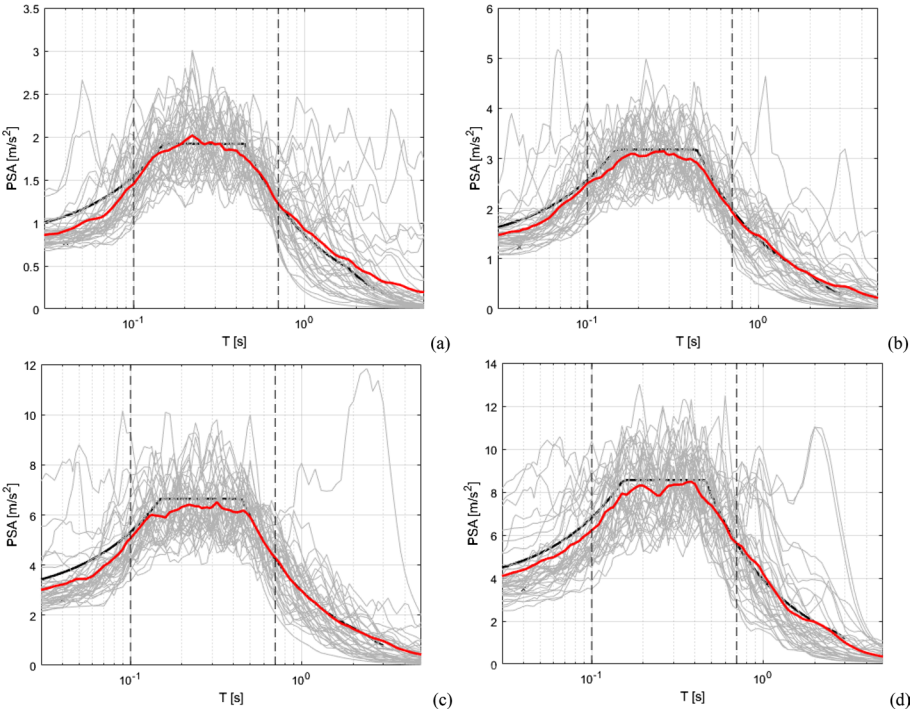

Fig. 13 Accelerogram selection related to the BT1_BM model for the damage states: **a** D_1, **b** D_2, **c** D_3, **d** D_4

actions, both components were adopted for the definition of the structural capacity, as described in Section 6.1.

6.1 Definition of the structural capacity

To carry out the fragility assessment of the typological structural models, it was first necessary to evaluate the ground-motion intensity ($PGA_i^{(j)}$) associated to the attainment of the j-th damage state for the i-th accelerogram. These PGA values, referred to as *structural capacity*, were computed by means of an iterative procedure. In particular, by finding, for the response spectrum of the i-th accelerogram, the scaling factor $SF_i^{(j)}$ that led to a displacement demand equal to the displacement capacity D_j, associated to the j-th damage state. Then the structural capacity in terms of PGA was computed as:

$$PGA_i^{(j)} = PGA_i \cdot SF_i^{(j)}, \tag{8}$$

where PGA_i is the PGA of the i-th accelerogram under consideration. This procedure was repeated for each permutation of the values of the mechanical properties, for each pushover analysis (i.e., for the different force distributions, directions and eccentricities) and for each of the two horizontal acceleration components of the ground-motion records and for both the displacement demand calculation methods (Guerrini et al. (2017) and CSM). A limit was imposed on the values of the scaling factors; namely, all the accelerograms associated to a scaling factor $SF_i^{(j)}$ lower than 0.5 or greater than 6 were neglected in the successive steps of the present work.

7 Fragility analysis

7.1 Response surface method

Response Surface (RS) models were used to define empirical relationships between structural capacity in terms of PGA and the random variables associated to the mechanical properties of the case study buildings. RSs were fitted to the observed data, i.e., the values of the structural capacity obtained from the different analyses carried out, aggregating the $PGA_i^{(j)}$ values for both the components of all accelerograms selected for the damage state D_j under consideration. Additionally, given the significant variability of the response variable, $PGA_i^{(j)}$, homogeneous k-th data groups were considered to define the RSs, i.e. separating the results according to the load distribution (either *uniform* or *modal),* loading direction ($\pm X$ or $\pm Y$) and displacement demand calculation method (Guerrini et al. (Guerrini et al. 2017) or CSM) considered in the analyses. A total of sixteen RSs for each damage state of each model was obtained. The RS functional forms adopted for the k-th data group of the models BT1_BM, BT2_SM and BT2_SM-BM were, respectively:

$$\ln(PGA_i^{(j,k)}) = a_1^{(j,k)} + a_2^{(j,k)} \ln(f_{m,b,i}) + a_3^{(j,k)} \ln(f_{v0,i}) + a_4^{(j,k)} \ln(E_{b,i}) + \varepsilon_i^{(j,k)}, \tag{9}$$

$$\ln(PGA_i^{(j,k)}) = b_1^{(j,k)} + b_2^{(j,k)} \ln(f_{m,s,i}) + b_3^{(j,k)} \ln(\tau_{0,s,i}) + b_4^{(j,k)} \ln(E_{s,i}) + \varepsilon_i^{(j,k)}, \tag{10}$$

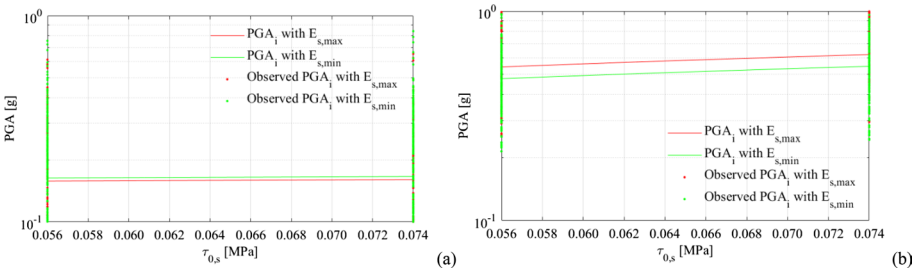

Fig. 14 Sections of RSs of the model BT2_SM for the data group with uniform distribution, $+X$ loading direction, Guerrini et al. Method for the limit states **a** D_1 and **b** D_4

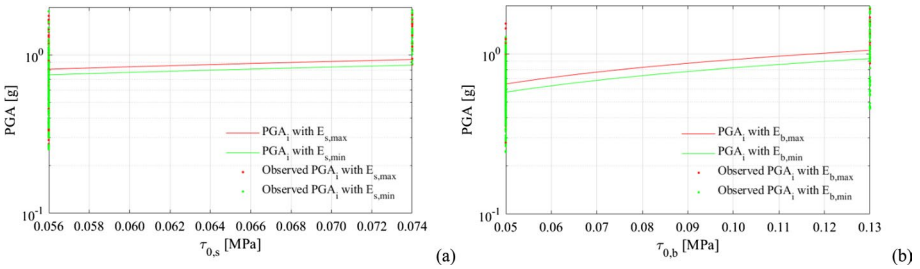

Fig. 15 Sections of RSs of the model BT2_SM-BM at the limit state D_4 for the data group with uniform distribution, + Y loading direction, Guerrini et al. Method considering the effect on the response of a variation in terms of shear strength of **a** stone masonry and **b** brick masonry

$$\begin{aligned}\ln\left(PGA_i^{(j,k)}\right) = {} & c_1^{(j,k)} + c_2^{(j,k)} \ln\left(f_{m,s,i}\right) + c_3^{(j,k)} \ln\left(\tau_{0,s,i}\right) \\ & + c_4^{(j,k)} \ln\left(E_{s,i}\right) + c_5^{(j,k)} \ln\left(f_{m,b,i}\right) \\ & + c_6^{(j,k)} \ln\left(\tau_{0,b,i}\right) + c_7^{(j,k)} \ln\left(E_{b,i}\right) + \varepsilon_i^{(j,k)},\end{aligned} \tag{11}$$

where $f_{m,b,i}$ and $f_{m,s,i}$ are the brick and stone masonry compressive strength, respectively, $\tau_{0,s,i}$, $\tau_{0,b,i}$ and $f_{v0,i}$ are the shear strength of brick or stone masonry, according to the shear failure criteria considered (see Section 3), $E_{b,i}$ and $E_{s,i}$ are the Young's modulus of brick and stone masonry, respectively, and $\varepsilon_i^{(j,k)}$ is a zero-mean normal error term with standard deviation $\sigma^2_{\varepsilon_i^{(j,k)}}$. The $a_1^{(j,k)}$, …, $a_4^{(j,k)}$, $b_1^{(j,k)}$, …, $b_4^{(j,k)}$, $c_1^{(j,k)}$, …, $c_7^{(j,k)}$ coefficients, associated, for each model, to the k-th data group and to the j-th damage state, and the standard deviation of the error term were estimated by means of linear regressions.

Sections of the Response Surfaces for the model BT2_SM are presented in Fig. 14. Among the sixteen RSs calibrated for this model, these sections were obtained by considering the data group with a uniform load distribution, a loading direction $+X$ and the Guerrini et al. Method. In more detail, Fig. 14a, b show the effect of a variation in terms of shear strength on the response, i.e., PGA for the damage states D_1 and D_4, respectively. These sections were evaluated by fixing the compressive strength of the stone masonry to its maximum value and by varying the Young's modulus, considering the minimum and the maximum values. It can be observed that a variation in terms of shear strength

influenced the response, i.e., lower shear strength values corresponded to lower PGA values, and that this effect was more significant for the damage state D_4, as expected. Sections of the Response Surfaces for the model BT2_SM-BM, accounting for the presence of two masonry typologies, are also reported in Fig. 15 for the combination with a uniform distribution, a loading direction + Y and the Guerrini et al. Method. The effects on the structural response given by variations in terms of shear strength for both the materials, i.e., stone masonry (Fig. 15a) and clay brick masonry (Fig. 15b), are here presented for the damage state D_4 only, and it was observed that they did influence the PGA values. In more detail, the effect on the structural response seemed more evident for the clay brick masonry, but it should be observed that a wider range for the shear strength was considered with respect to stone masonry, according to Table 1.

The RS models provided analytical estimates of the values of the structural capacity in terms of PGA, as a function of the random variables associated to the material properties, representing also the uncertainty related to the structural response to different ground-motions. Therefore, the RS models can be efficiently adopted to compute the exceedance probability of a damage state D_j as a function of the seismic demand, defined in terms of PGA.

7.2 Derivation of fragility curves

The random variables used to represent uncertainties on material properties were assumed to follow lognormal distributions, with the parameters reported in Table 4. These were derived from the CNR DT212/2013 Guidelines (CNR-DT212/2013 2014), while the values referring to fv_0 were obtained in a previous research (Ferretti et al. 2016, 2019), devoted to the investigation of the mechanical properties of existing masonry buildings, similar to the ones here considered and located in the Emilia Romagna region.

Once the unknown coefficients in Eqs. (9–11) were determined, it was straightforward, for the k-th data group of each model, to compute the mean and the variance of the PGA capacity for the D_j damage state. This was done by considering Eq. (12), Eq. (13) or Eq. (14) for the models BT1_BM, BT2_SM and BT2_SM-BM, respectively:

$$\begin{aligned}\mu_{\ln\left(PGA_i^{(j,k)}\right)} &= a_1^{(j,k)} + a_2^{(j,k)} \ln\left(\mu_{f_{m,b,i}}\right) + a_3^{(j,k)} \ln\left(\mu_{f_{v0,i}}\right) + a_4^{(j,k)} \ln\left(\mu_{E_{b,i}}\right) \\ \sigma^2_{\ln\left(PGA_i^{(j,k)}\right)} &= {a_2^{(j,k)}}^2 \sigma^2_{\ln(f_{m,b,i})} + {a_3^{(j,k)}}^2 \sigma^2_{\ln(f_{v0,i})} + {a_4^{(j,k)}}^2 \sigma^2_{\ln(E_{b,i})} + \sigma^2_{\varepsilon_i^{(j,k)}}\end{aligned}, \tag{12}$$

$$\begin{aligned}\mu_{\ln(PGA_i^{(j,k)})} &= b_1^{(j,k)} + b_2^{(j,k)} \ln\left(\mu_{f_{m,s,i}}\right) + b_3^{(j,k)} \ln\left(\mu_{\tau_{0,s,i}}\right) + b_4^{(j,k)} \ln\left(\mu_{E_{s,i}}\right) \\ \sigma^2_{\ln(PGA_i^{(j,k)})} &= b_2^{(j,k)^2} \sigma^2_{\ln(f_{m,s,i})} + b_3^{(j,k)^2} \sigma^2_{\ln(\tau_{0,s,i})} + b_4^{(j,k)^2} \sigma^2_{\ln(E_{s,i})} + \sigma^2_{\varepsilon_i^{(j,k)}}\end{aligned}, \tag{13}$$

Table 4 Mean value and logarithmic standard deviation for the mechanical parameters

Masonry typology		f_m (MPa)	τ_0 (MPa)	f_{v0} (MPa)	E (MPa)
Clay brick with lime-based mortar	μ	3.20	0.076	0.155	1500
	$\sigma_{(ln)}$	0.0026	0.0021	0.0060	0.0020
Stone masonry with regular bond pattern	μ	3.20	0.065	–	1740
	$\sigma_{(ln)}$	0.0019	0.0014	–	0.0014

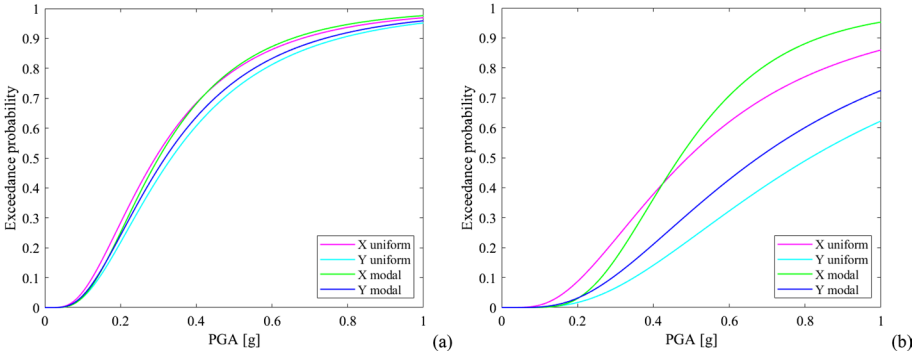

Fig. 16 Model BT1_BM—Lognormal fragility curves in terms of PGA for the damage states **a** D_2 and **b** D_4

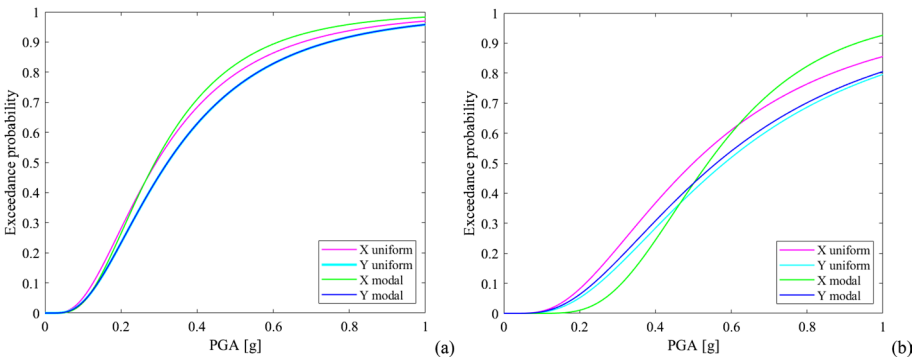

Fig. 17 Model BT2_SM—Lognormal fragility curves in terms of PGA for the damage states **a** D_2 and **b** D_4

$$\begin{aligned}\mu_{\ln(PGA_i^{(j,k)})} &= c_1^{(j,k)} + c_2^{(j,k)}\ln(\mu_{f_{m,s,i}}) + c_3^{(j,k)}\ln(\mu_{\tau_{0,s,i}}) + c_4^{(j,k)}\ln(\mu_{E_{s,i}}) + c_5^{(j,k)}\ln(\mu_{f_{m,b,i}}) + c_6^{(j,k)}\ln(\mu_{\tau_{0,b,i}}) + c_7^{(j,k)}\ln(\mu_{E_{b,i}}) \\ \sigma^2_{\ln(PGA_i^{(j,k)})} &= c_2^{(j,k)^2}\sigma^2_{\ln(f_{m,s,i})} + c_3^{(j,k)^2}\sigma^2_{\ln(\tau_{0,s,i})} + c_4^{(j,k)^2}\sigma^2_{\ln(E_{s,i})} + c_5^{(j,k)^2}\sigma^2_{\ln(f_{m,b,i})} + c_6^{(j,k)^2}\sigma^2_{\ln(\tau_{0,b,i})} + c_7^{(j,k)^2}\sigma^2_{\ln(E_{b,i})} + \sigma^2_{\varepsilon_i^{(j,k)}}\end{aligned} \tag{14}$$

Assuming that the natural logarithm of the PGA capacity is normally distributed with mean $\mu_{\ln(PGA_i^{(j,k)})}$ and standard deviation $\sigma_{\ln(PGA_i^{(j,k)})}$, the probability of exceedance for the k-th data group of each model and for each damage state D_j was computed as:

$$p^{(j,k)} = \Phi\left(\frac{\ln(PGA_i^{(j,k)}) - \mu_{\ln(PGA_i^{(j,k)})}}{\sigma_{\ln(PGA_i^{(j,k)})}}\right) \tag{15}$$

7.3 Fragility curves

Depending on the loading direction, the force distribution, and the displacement demand calculation method, sixteen sets of fragility curves were obtained for the considered models. Few examples of the fragility curves obtained using the Guerrini et al. method

(Guerrini et al. 2017) are presented in Figs. 16 and 17 for the model BT1_BM and BT2_SM, respectively. The influence of the force distribution and of the loading direction on the fragility curves for brick and stone masonry and for the damage states D_2 and D_4 was evidenced. The most significant differences were observed for the damage state D_4. For this representation, positive and negative X and Y directions were considered together.

In the present paper, the approach proposed by Shinozuka et al. (2000) to combine fragility curves was adopted. In particular, being M the total number of k-th data groups, it was considered:

$$\begin{aligned}
&\mu_{\ln(PGA^{(j)})} = \sum_{k=1}^{M} P_k \mu_{\ln(PGA_i^{(j,k)})} j = 1, ..., 4 \\
&\sigma^2_{\ln(PGA^{(j)})} = P^T \Sigma + A^T Q A \\
&P^T = [P_1, ..., P_M] \\
&\Sigma = [\sigma^2_{\ln(PGA_i^{(j,k=1)})}, ..., \sigma^2_{\ln(PGA_i^{(j,k=M)})}] \\
&A^T = [\mu_{\ln(PGA_i^{(j,k=1)})}, ..., \mu_{\ln(PGA_i^{(j,k=M)})}] \\
&Q = \begin{bmatrix} P_1(1-P_1) & -P_1P_2 & \dots & -P_1P_2 \\ \vdots & & & \\ -P_MP_1 & -P_MP_2 & \dots & P_M(1-P_M) \end{bmatrix}
\end{aligned} \tag{16}$$

Given that the k-th data groups were equally populated, $P_h = 1/M$ was the weight assigned to each group. As suggested in the cited work (Shinozuka et al. 2000), the combined fragility curves may be assumed to be lognormal with respect to the mean $\mu_{\ln(PGA^{(j)})}$ and the variance $\sigma^2_{\ln(PGA^{(j)})}$ can be estimated on the basis of the variances of the single fragility curves, see Eqs. (12–14, 16).

The described approach was first applied considering separately the fragility curves obtained from the two displacement demand computation methods ($M = 8$). In this way, combined fragility curves were obtained, two for each model, independent from the loading direction and the shape of the load distribution. As an example, the fragility curves for the model BT1_BM are reported in Fig. 18. It can be observed that the two sets of curves

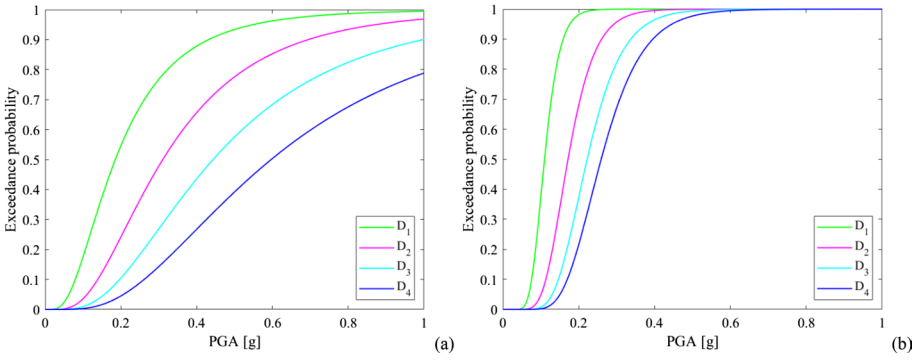

Fig. 18 Fragility curves for BT1_BM in terms of PGA for four different damage states: **a** Guerrini et al. Method, **b** CSM

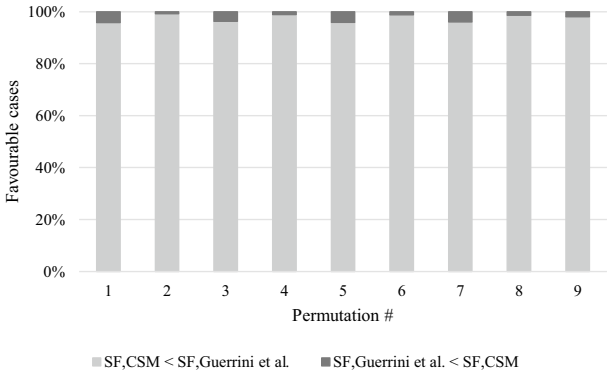

Fig. 19 Percentages of scale factors computed with the CSM that are lower than the corresponding value obtained with the Guerrini et al. Method, and vice versa, for BT1_BM at damage limit state D_4

Table 5 Parameters of the combined lognormal fragility curves

Model	Parameter	D_1	D_2	D_3	D_4
BT1_BM	μ_{ln}	−1.947	−1.465	−1.159	−0.933
	σ_{ln}	0.571	0.587	0.618	0.667
BT2_SM	μ_{ln}	−1.921	−1.404	−1.136	−0.917
	σ_{ln}	0.580	0.574	0.610	0.660
BT2_SM-BM	μ_{ln}	−1.890	−1.300	−1.083	−0.827
	σ_{ln}	0.589	0.584	0.589	0.645

were quite dissimilar. This can be explained by evaluating the percentage of ground-motion scale factors derived by implementing the Capacity Spectrum Method which were lower or higher than the corresponding values obtained through the Guerrini et al. method. This was done for all the permutations, the analyses and the accelerogram horizontal components considered. Results are representatively presented in Fig. 19 for the model BT1_BM at the damage limit state D_4, for which, in most cases, the lowest scale factors were obtained through the Capacity Spectrum Method. Similar observations can be coherently applied to all other damage limit states and to all the structural models. Therefore, it can be highlighted that the PGA capacity computed from the Capacity Spectrum Method, according to Eq. (8), was systematically lower compared to the same value obtained by implementing the Guerrini et al. method.

The displacement demand calculation method, as observed, represent one of the different sources of uncertainties involved in the problem. Then, with the objective of obtaining fragility curves independent from the displacement demand calculation method, as well as from the loading direction and the shape of the load distribution, the Shinozuka's approach (Shinozuka et al. 2000) was eventually applied combining the fragility curves obtained for all the k-th data groups of each model, for each damage state ($M = 16$). The parameters (μ_{ln}, σ_{ln}) of the combined fragility curves are reported in Table 5, while the curves are presented in Fig. 20 for the three typological buildings.

Figure 21 shows an attempt of comparing the fragility curves with others obtained in the literature, both analytically and empirically, for similar building typologies. To this aim, the curves obtained for the model BT1_BM (i.e., brick masonry typology) are considered; the other models are not considered because their features do not find a direct match in the

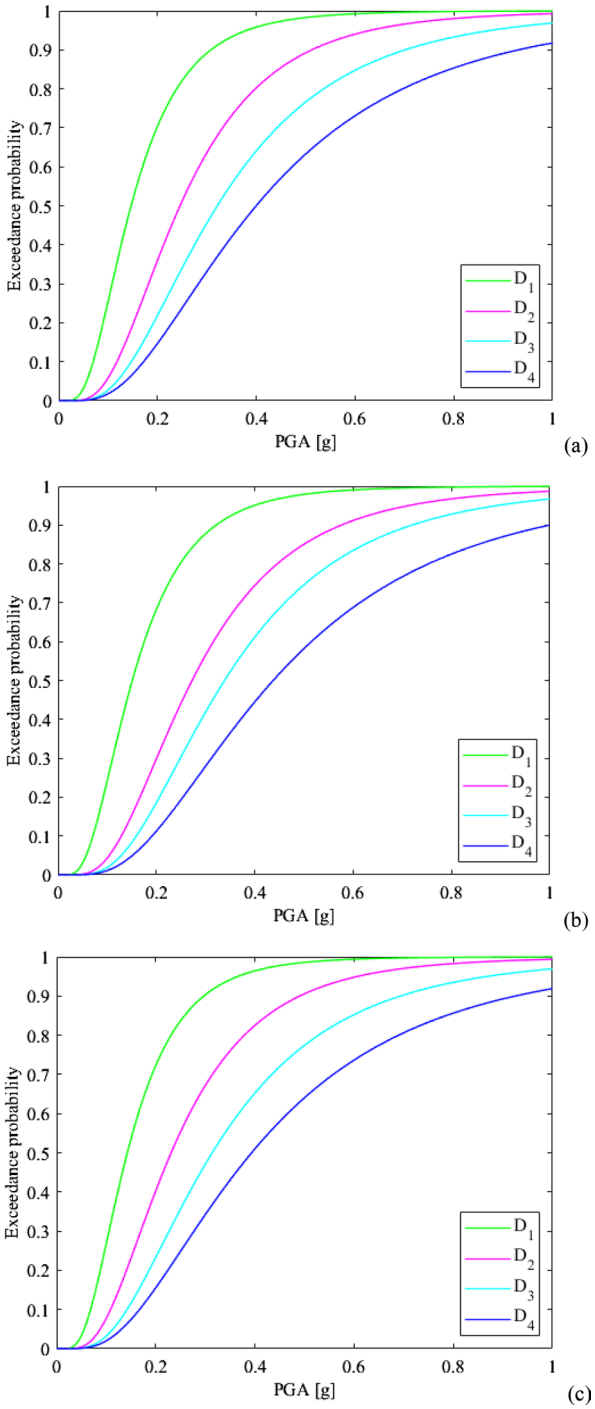

Fig. 20 Combined fragility curves in terms of PGA for four different damage states for the model: **a** BT1_BM, **b** BT2_SM, **c** BT2_SM-BM

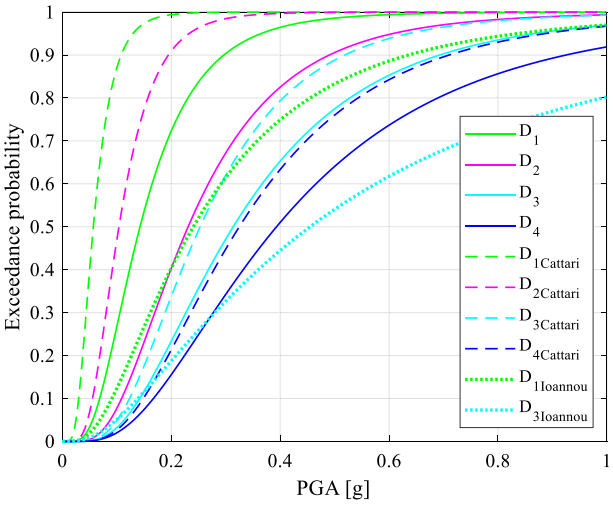

Fig. 21 Comparison of fragility curves obtained for the model BT1_BM with analytical (Cattari et al. 2014) and empirical (Ioannou et al. 2021) ones

literature. In the comparison, the analytical fragility curves were obtained for unreinforced clay brick masonry buildings, characterized by a regular plan and elevation configuration and by the presence of rigid concrete floors (Cattari et al. 2014; Lagomarsino and Cattari 2014). The definition of damage states (D_1 to D_4) was compatible with the one adopted in the present work with the addition of further drift limits. Differences between the fragility curves can be observed especially for the damage state D_2 and can be attributed to differences in the structural configuration of the considered buildings (e.g., deformable *vs* rigid slab) and to possible discrepancies in the identification of the different damage states, in particular due to drift limits.

The empirical curves were derived from a recent work (Ioannou et al. 2021), focused on RC and masonry buildings of the Emilia-Romagna Region. In this case, the comparison was only made for damage states D_1 and D_3, since limited observational data were obtained for D_4 and D_5 in the cited work. It can be noticed that analytical models feature an higher fragility than empirical models, this is due to the criteria adopted for the definition of the damage states and to the modeling assumptions. Actual buildings normally have a higher dissipative capacity than numerical models because these latter introduce various simplifications of the mechanical behavior of materials and structural elements and do not consider the contribution of non-structural elements.

8 Conclusions

This paper presented a methodology to analytically assess the fragility of typological unreinforced masonry buildings. To this aim, two case study buildings, representative of part of the building stock of the Emilia Romagna region, were identified: their construction details and geometry were selected from a statistical analysis of both the 2011 census data and the post-earthquake surveys database from the 2012 Emilia earthquake. Based on the selected case studies, three tri-dimensional models were considered to investigate the behaviour of different building typologies, i.e., with stone masonry, brick masonry or both.

The capacity of these structures was computed by means of pushover analyses and damage states were identified according to literature indications. Moreover, several permutations of the mechanical parameters were implemented to account for the variability of the masonry mechanical properties, according to the Design of Experiments theory. Local failure modes were not analysed.

To consider the variability of the seismic action, ground motion recordings were selected from the PEER Ground motion database. The displacement demand was then calculated by means of two different displacement demand calculation methods, derived both from building codes and available literature: the N2 Method, as modified by Guerrini et al. (2017), and the Capacity Spectrum Method. Response Surfaces were fitted to the observed data to estimate the structural capacity, in terms of PGA, as a function of the mechanical properties of masonry, assumed as random variables. It was observed that the parameter mostly affecting the structural response was the masonry shear strength, coherently with the failure modes obtained in the nonlinear static analyses.

Fragility curves were then obtained for homogenous groups of data, aggregating the results, in terms of PGA capacity, according to the displacement demand calculation method, the load distribution and the loading direction. These sets of curves were then combined, obtaining overall lognormal fragility curves for each building and for each damage limit state. A critical comparison with analytical and empirical fragility curves was also presented for the brick masonry typology.

In conclusion, the proposed methodology allowed to thoroughly consider the uncertainties related to the mechanical properties of masonry as well as to the seismic action and the displacement demand calculation method. Based on the use of Response Surface to perform the fragility assessment, it can be successfully applied for the determination of typological fragility curves for URM buildings, as demonstrated by its application to the case studies presented in this research.

Appendix

A. 1 Selected accelerograms for model BT1_BM at damage state D_1

Earthquake name	Year	Station name	Moment magnitude M_w (−)	Joyner-Boore distance (km)	$V_{S,30}$ (m/s)
Mammoth Lakes-07	1980	Fish & Game (FIS)	4.73	3.33	373.2
Imperial Valley-07	1979	Calexico Fire Station	5.01	11.17	231.2
Hollister-03	1974	San Juan Bautista, 24 Polk St	5.14	8.56	335.5
Northern Calif-07	1975	Ferndale City Hall	5.20	8.20	219.3
Calabria, Italy	1978	Ferruzzano	5.20	8.13	525.6
Whittier Narrows-02	1987	Bell Gardens–Jaboneria	5.27	9.92	267.1
Whittier Narrows-02	1987	LA–N Figueroa St	5.27	8.00	364.9
Northridge-06	1994	Hollywood–Willoughby Ave	5.28	16.25	347.7
Umbria Marche (aftershock 2), Italy	1997	Cascia	5.60	19.92	585.0

Earthquake name	Year	Station name	Moment magnitude M_w (−)	Joyner-Boore distance (km)	$V_{S,30}$ (m/s)
Umbria Marche (aftershock 2), Italy	1997	Norcia-Zona Industriale	5.60	17.69	551.0
L'Aquila (aftershock 1), Italy	2009	L'Aquila–Parking	5.60	5.07	717.0
Point Mugu	1973	Port Hueneme	5.65	15.48	249.0
Mammoth Lakes-05	1980	Convict Creek	5.70	6.06	382.1
Taiwan SMART1(5)	1981	SMART1 I06	5.90	25.31	309.4
Taiwan SMART1(5)	1981	SMART1 O07	5.90	23.77	314.3
Double Springs	1994	Woodfords	5.90	12.48	393.0
Taiwan SMART1(5)	1981	SMART1 O10	5.90	26.66	320.1
Morgan Hill	1984	Hollister Differential Array #3	6.19	26.42	215.5
Chalfant Valley-02	1986	Long Valley Dam (L Abut)	6.19	18.30	537.2
Irpinia, Italy-02	1980	Sturno (STN)	6.20	20.38	382.0
Chi-Chi, Taiwan-03	1999	CHY029	6.20	31.08	544.7
Chi-Chi, Taiwan-03	1999	TCU089	6.20	5.93	671.5
Chi-Chi, Taiwan-04	1999	CHY087	6.20	38.32	505.2
Chi-Chi, Taiwan-05	1999	HWA034	6.20	32.57	379.2
Christchurch, New Zealand	2011	ASHS	6.20	30.46	295.7
Christchurch, New Zealand	2011	CSTC	6.20	36.18	332.7
Chi-Chi, Taiwan-06	1999	TCU109	6.30	36.58	535.1
Chi-Chi, Taiwan-06	1999	TCU123	6.30	38.26	270.2
Victoria, Mexico	1980	SAHOP Casa Flores	6.33	39.10	259.6
Coalinga-01	1983	Parkfield–Vineyard Cany 1W	6.36	27.72	284.2
Northridge-01	1994	Leona Valley #1	6.69	36.86	499.3
Northridge-01	1994	Leona Valley #3	6.69	37.00	499.3
Kobe, Japan	1995	OSAJ	6.90	21.35	256.0
Darfield, New Zealand	2010	LRSC	7.00	9.38	295.7
El Mayor-Cucapah	2010	Sam W. Stewart	7.20	31.79	503.0
Chi-Chi, Taiwan	1999	CHY082	7.62	36.09	193.7
Chi-Chi, Taiwan	1999	TCU112	7.62	27.48	190.5
Chi-Chi, Taiwan	1999	TCU113	7.62	31.05	230.3
Chi-Chi, Taiwan	1999	TCU141	7.62	24.19	223.0
Chi-Chi, Taiwan	1999	TCU145	7.62	35.32	240.4

A. 2 Selected accelerograms for model BT1_BM at damage state D_2

Earthquake name	Year	Station name	Moment magnitude M_w (-)	Joyner-Boore distance (km)	$V_{S,30}$ (m/s)
Imperial Valley-07	1979	El Centro Array #11	5.01	13.61	196.3
Hollister-03	1974	Hollister City Hall	5.14	8.85	198.8
Whittier Narrows-02	1987	LA–116th St School	5.27	19.12	301.0
Lytle Creek	1970	Wrightwood–6074 Park Dr	5.33	10.70	486.0
Chalfant Valley-04	1986	Bishop–LADWP South St	5.44	23.99	303.5
Umbria Marche (aftershock 1), Italy	1997	Nocera Umbra-Salmata	5.50	11.72	694.0
Mt. Lewis	1986	Halls Valley	5.60	12.37	281.6
Lazio Abruzzo, Italy	1984	Cassino-Sant' Elia	5.80	19.97	436.8
Chi-Chi, Taiwan-02	1999	TCU074	5.90	4.14	549.4
Whittier Narrows-01	1987	Brea–S Flower Av	5.99	18.39	322.8
Whittier Narrows-01	1987	Panorama City–Roscoe	5.99	32.13	318.2
Umbria Marche, Italy	1997	Castelnuovo-Assisi	6.00	17.28	293.0
N. Palm Springs	1986	Cranston Forest Station	6.06	27.21	425.2
Chi-Chi, Taiwan-03	1999	TCU072	6.20	21.18	468.1
Chi-Chi, Taiwan-04	1999	CHY046	6.20	38.11	442.2
Chi-Chi (aftershock 3), Taiwan	1999	CHY006	6.20	24.58	438.2
Chi-Chi, Taiwan-06	1999	CHY024	6.30	29.49	427.7
Chi-Chi, Taiwan-06	1999	CHY028	6.30	32.09	542.6
Chi-Chi, Taiwan-06	1999	CHY101	6.30	34.55	258.9
Chi-Chi, Taiwan-06	1999	TCU122	6.30	29.64	475.5
Imperial Valley-06	1979	Compuertas	6.53	13.52	259.9
Imperial Valley-06	1979	El Centro Array #12	6.53	17.94	196.9
Imperial Valley-06	1979	Parachute Test Site	6.53	12.69	348.7
Niigata, Japan	2004	FKS028	6.63	30.11	305.5
Northridge-01	1994	LA–Pico & Sentous	6.69	27.82	304.7
Northridge-01	1994	LA–S. Vermont Ave	6.69	27.89	301.9
Northridge-01	1994	LA–W 15th St	6.69	25.59	329.5
Northridge-01	1994	Manhattan Beach–Manhattan	6.69	33.56	351.6
Chuetsu-oki	2007	Nadachiku Joetsu City	6.80	35.79	570.6
Chuetsu-oki	2007	Mitsuke Kazuiti Arita Town	6.80	11.35	274.2
Chuetsu-oki	2007	Hinodecho Yoshida Tsubame City	6.80	20.44	261.6
Iwate	2008	Kami, Miyagi Miyazaki City	6.90	25.15	477.6
Iwate	2008	Sanbongi Osaki City	6.90	36.33	539.9
Iwate	2008	Hirakamachi Asamai Yokote	6.90	34.76	325.8
Loma Prieta	1989	Fremont–Emerson Court	6.93	39.66	284.8
Loma Prieta	1989	Fremont–Mission San Jose	6.93	39.32	367.6
Darfield, New Zealand	2010	OXZ	7.00	30.63	481.6
Landers	1992	North Palm Springs	7.28	26.84	344.7

Earthquake name	Year	Station name	Moment magnitude M_w (-)	Joyner-Boore distance (km)	$V_{S,30}$ (m/s)
Landers	1992	North Palm Springs Fire Sta #36	7.28	26.95	367.8
Chi-Chi, Taiwan	1999	TCU048	7.62	13.53	551.2

A. 3 Selected accelerograms for model BT1_BM at damage state D_3

Earthquake name	Year	Station name	Moment magnitude M_w (-)	Joyner-Boore distance (km)	$V_{S,30}$ (m/s)
Chalfant Valley-01	1986	Zack Brothers Ranch	5.77	6.07	316.2
Northwest China-01	1997	Jiashi	5.90	12.62	240.1
Whittier Narrows-01	1987	Compton–Castlegate St	5.99	18.32	266.9
Whittier Narrows-01	1987	San Gabriel–E Grand Ave	5.99	0.00	401.4
Parkfield-02, CA	2004	PARKFIELD–HOG CANYON	6.00	0.73	363.7
Parkfield-02, CA	2004	PARKFIELD–VINEYARD CANYON	6.00	4.36	340.5
Parkfield-02, CA	2004	Parkfield–Cholame 4AW	6.00	4.81	283.4
Parkfield-02, CA	2004	PARKFIELD–UPSAR 05	6.00	9.14	440.6
Parkfield-02, CA	2004	Hog Canyon	6.00	4.51	376.0
Mammoth Lakes-01	1980	Long Valley Dam (Upr L Abut)	6.06	12.56	537.2
Northwest China-03	1997	Jiashi	6.10	9.98	240.1
Kalamata, Greece-01	1986	Kalamata (bsmt)	6.20	6.45	382.2
L'Aquila, Italy	2009	L'Aquila–V. Aterno -Colle Grilli	6.30	0.00	685.0
Imperial Valley-06	1979	Calexico Fire Station	6.53	10.45	231.2
Imperial Valley-06	1979	Delta	6.53	22.03	242.1
Superstition Hills-02	1987	El Centro Imp. Co. Cent	6.54	18.20	192.1
Superstition Hills-02	1987	Westmorland Fire Sta	6.54	13.03	193.7
New Zealand-02	1987	Matahina Dam	6.60	16.09	551.3
San Fernando	1971	Castaic–Old Ridge Route	6.61	19.33	450.3
Niigata, Japan	2004	NIG023	6.63	25.33	654.8
Northridge-01	1994	Arleta–Nordhoff Fire Sta	6.69	3.3	297.7
Northridge-01	1994	LA–S Grand Ave	6.69	29.52	285.3
Chuetsu-oki	2007	Joetsu Yanagishima paddocks	6.80	28.07	605.7
Chuetsu-oki	2007	Sanjo Shinbori	6.80	15.89	278.1
Chuetsu-oki	2007	Tani Kozima Nagaoka	6.80	5.00	561.6
Chuetsu-oki	2007	Kariwa	6.80	0.00	282.6
Kobe, Japan	1995	Kakogawa	6.90	22.50	312.0
Iwate	2008	Mizusawaku Interior O ganecho	6.90	7.82	413.0
Loma Prieta	1989	Anderson Dam (Downstream)	6.93	19.90	488.8
Imperial Valley-02	1940	El Centro Array #9	6.95	6.09	213.4
Darfield, New Zealand	2010	Christchurch Cashmere High School	7.00	17.64	204.0
Hector Mine	1999	Hector	7.13	10.35	726.0

Earthquake name	Year	Station name	Moment magnitude M_w (-)	Joyner-Boore distance (km)	$V_{S,30}$ (m/s)
El Mayor-Cucapah	2010	Chihuahua	7.20	18.21	242.1
El Mayor-Cucapah	2010	CERRO PRIETO GEOTHERMAL	7.20	8.88	242.1
El Mayor-Cucapah	2010	Bonds Corner	7.20	30.75	223.0
El Mayor-Cucapah	2010	Calexico Fire Station	7.20	19.12	231.2
El Mayor-Cucapah	2010	El Centro Array #7	7.20	27.42	210.5
Chi-Chi, Taiwan	1999	TCU055	7.62	6.34	359.1
Chi-Chi, Taiwan	1999	TCU089	7.62	0.00	671.5
Wenchuan, China	2008	Anxiantashui	7.90	0.00	376.1

A.4 Selected accelerograms for model BT1_BM at damage state D_4

Earthquake name	Year	Station name	Moment magnitude M_w (-)	Joyner-Boore distance (km)	$V_{S,30}$ (m/s)
Yountville	2000	Napa Fire Station #3	5.00	8.48	328.6
Mammoth Lakes-06	1980	Long Valley Dam (Upr L Abut)	5.94	9.65	537.2
Whittier Narrows-01	1987	Downey–Birchdale	5.99	14.90	245.1
Parkfield-02, CA	2004	Parkfield–Fault Zone 3	6.00	1.10	211.7
Parkfield-02, CA	2004	PARKFIELD–UPSAR 07	6.00	9.14	440.6
Parkfield-02, CA	2004	PARKFIELD–UPSAR 11	6.00	8.93	466.1
N. Palm Springs	1986	Desert Hot Springs	6.06	0.99	359.0
Parkfield	1966	Cholame–Shandon Array #5	6.19	9.58	289.6
Morgan Hill	1984	Anderson Dam (Downstream)	6.19	3.22	488.8
Christchurch, New Zealand	2011	Christchurch Cashmere High School	6.20	4.44	204.0
Christchurch, New Zealand	2011	Shirley Library	6.20	5.58	207.0
Managua, Nicaragua-01	1972	Managua, ESSO	6.24	3.51	288.8
L'Aquila, Italy	2009	L'Aquila–V. Aterno -Colle Grilli	6.30	0.00	685.0
Victoria, Mexico	1980	Cerro Prieto	6.33	13.80	471.5
Coalinga-01	1983	Pleasant Valley P.P.–bldg	6.36	7.69	257.4
Friuli, Italy-01	1976	Tolmezzo	6.50	14.97	505.2
Imperial Valley-06	1979	Delta	6.53	22.03	242.1
Superstition Hills-02	1987	Poe Road (temp)	6.54	11.16	316.6
Niigata, Japan	2004	NIG023	6.63	25.33	654.8
Erzican, Turkey	1992	Erzincan	6.69	0.00	352.1
Northridge-01	1994	Canoga Park–Topanga Can	6.69	0.00	267.5
Northridge-01	1994	LA–Hollywood Stor FF	6.69	19.73	316.5
Northridge-01	1994	Los Angeles–7-story Univ Hospital (FF)	6.69	32.39	332.3
Northridge-01	1994	LA 00	6.69	9.87	706.2
Northridge-01	1994	Sun Valley–Roscoe Blvd	6.69	5.59	320.9
Chuetsu-oki	2007	Yoshikawaku Joetsu City	6.80	13.68	561.6

Earthquake name	Year	Station name	Moment magnitude M_w (-)	Joyner-Boore distance (km)	$V_{S,30}$ (m/s)
Chuetsu-oki	2007	Kashiwazaki City Center	6.80	0.00	294.4
Chuetsu-oki	2007	Yoitamachi Yoita Nagaoka	6.80	4.69	655.5
Chuetsu-oki	2007	Kawanishi Izumozaki	6.80	0.00	338.3
Chuetsu-oki	2007	NIG018	6.80	0.00	198.3
Loma Prieta	1989	Gilroy–Gavilan Coll	6.93	9.19	729.7
Darfield, New Zealand	2010	DFHS	7.00	11.86	344.0
Darfield, New Zealand	2010	Kaiapoi North School	7.00	30.53	255.0
El Mayor-Cucapah	2010	MICHOACAN DE OCAMPO	7.20	13.21	242.1
El Mayor-Cucapah	2010	El Centro–Imperial & Ross	7.20	19.39	229.3
Tabas, Iran	1978	Dayhook	7.35	0.00	471.5
Chi-Chi, Taiwan	1999	TCU067	7.62	0.62	433.6
Chi-Chi, Taiwan	1999	TCU089	7.62	0.00	671.5
Wenchuan, China	2008	Jiangyouchonghua	7.90	27.23	430.5
Wenchuan, China	2008	Anxiantashui	7.90	0.00	376.1

B.1 Selected accelerograms for models BT2_SM and BT2_SM-BM at damage state D_1

Earthquake name	Year	Station name	Moment magnitude M_w (-)	Joyner-Boore distance (km)	$V_{S,30}$ (m/s)
Imperial Valley-07	1979	El Centro Array #2	5.01	17.32	188.8
Imperial Valley-07	1979	El Centro Array #8	5.01	8.18	206.1
Coalinga-02	1983	TRA (temp)	5.09	6.64	246.5
Coalinga-02	1983	VEW (temp)	5.09	1.89	456.1
Whittier Narrows-02	1987	Inglewood–Union Oil	5.27	22.21	316.0
Whittier Narrows-02	1987	LA–116th St School	5.27	19.12	301.0
Hollister-04	1986	Hollister Differential Array #3	5.45	13.11	215.5
Coyote Lake	1979	San Juan Bautista, 24 Polk St	5.74	19.46	335.5
Taiwan SMART1(5)	1981	SMART1 I03	5.90	25.49	314.9
Taiwan SMART1(5)	1981	SMART1 I09	5.90	25.51	309.4
Whittier Narrows-01	1987	Brea–S Flower Av	5.99	18.39	322.8
Parkfield-02, CA	2004	Parkfield–Gold Hill 1W	6.00	0.80	214.4
Parkfield-02, CA	2004	Parkfield–Vineyard Cany 4W	6.00	6.74	386.2
Irpinia, Italy-02	1980	Rionero In Vulture	6.20	22.68	574.9
Chi-Chi, Taiwan-03	1999	CHY025	6.20	27.88	277.5
Chi-Chi, Taiwan-04	1999	CHY046	6.20	38.11	442.2
Chi-Chi (aftershock 3), Taiwan	1999	CHY006	6.20	24.58	438.2
Christchurch, New Zealand	2011	LINC	6.20	18.47	263.2
Christchurch, New Zealand	2011	TPLC	6.20	16.60	249.3

Earthquake name	Year	Station name	Moment magnitude M_w (-)	Joyner-Boore distance (km)	$V_{S,30}$ (m/s)
Chi-Chi, Taiwan-06	1999	CHY025	6.30	39.07	277.5
Coalinga-01	1983	Parkfield–Stone Corral 3E	6.36	32.81	565.1
Big Bear-01	1992	San Bernardino–2nd & Arrowhead	6.46	33.56	325.8
San Simeon, CA	2003	San Antonio Dam–Toe	6.52	16.17	509.0
Superstition Hills-02	1987	Brawley Airport	6.54	17.03	208.7
San Fernando	1971	Pasadena–CIT Athenaeum	6.61	25.47	415.1
Northridge-01	1994	Alhambra–Fremont School	6.69	35.66	549.8
Northridge-01	1994	Arcadia–Arcadia Av	6.69	39.41	330.5
Northridge-01	1994	LA–S. Vermont Ave	6.69	27.89	301.9
Northridge-01	1994	LA–W 15th St	6.69	25.59	329.5
Northridge-01	1994	Malibu–Point Dume Sch	6.69	26.77	349.5
Irpinia, Italy-01	1980	Rionero In Vulture	6.90	27.49	574.9
Iwate	2008	Sanbongi Osaki City	6.90	36.33	539.9
Iwate	2008	Yokote Masuda Tamati Masu	6.90	27.24	368.3
Iwate	2008	Yokote Ju Monjimachi	6.90	30.15	343.7
Iwate	2008	Ugo Town–Nishimonai	6.90	37.08	317.4
Darfield, New Zealand	2010	ADCS	7.00	28.46	249.3
Cape Mendocino	1992	Fortuna–Fortuna Blvd	7.01	15.97	457.1
Landers	1992	Mission Creek Fault	7.28	26.96	355.4
Landers	1992	Thousand Palms Post Office	7.28	36.93	333.9
Tabas, Iran	1978	Boshrooyeh	7.35	24.07	324.6

B.2 Selected accelerograms for models BT2_SM and BT2_SM-BM at damage state D_2

Earthquake name	Year	Station name	Moment magnitude M_w (-)	Joyner-Boore distance (km)	$V_{S,30}$ (m/s)
Imperial Valley-07	1979	Holtville Post Office	5.01	7.69	202.9
Hollister-03	1974	Hollister City Hall	5.14	8.85	198.8
Northridge-06	1994	Pacoima Kagel Canyon	5.28	10.21	508.1
Lytle Creek	1970	Wrightwood–6074 Park Dr	5.33	10.70	486.0
Mammoth Lakes-10	1983	Convict Creek	5.34	6.50	382.1
Livermore-02	1980	San Ramon–Eastman Kodak	5.42	14.31	377.5
Chalfant Valley-04	1986	Bishop–LADWP South St	5.44	23.99	303.5
Mt. Lewis	1986	Halls Valley	5.60	12.37	281.6
Mammoth Lakes-02	1980	Convict Creek	5.69	2.91	382.1
Mammoth Lakes-04	1980	Long Valley Dam (Upr L Abut)	5.70	12.75	537.2
Whittier Narrows-01	1987	LA–Baldwin Hills	5.99	21.51	297.1
Whittier Narrows-01	1987	N Hollywood–Coldwater Can	5.99	28.37	326.5

Earthquake name	Year	Station name	Moment magnitude M_w (-)	Joyner-Boore distance (km)	$V_{S,30}$ (m/s)
Whittier Narrows-01	1987	Pasadena–CIT Bridge Lab	5.99	4.30	341.1
Joshua Tree, CA	1992	North Palm Springs Fire Sta #36	6.10	21.40	367.8
Irpinia, Italy-02	1980	Calitri	6.20	8.81	455.9
Chi-Chi, Taiwan-03	1999	TCU075	6.20	18.47	573.0
Chi-Chi, Taiwan-04	1999	CHY101	6.20	21.62	258.9
Christchurch, New Zealand	2011	Styx Mill Transfer Station	6.2	11.24	247.5
Chi-Chi, Taiwan-06	1999	CHY028	6.30	32.09	542.6
Chi-Chi, Taiwan-06	1999	CHY101	6.30	34.55	258.9
San Simeon, CA	2003	Cambria–Hwy 1 Caltrans Bridge	6.5	6.97	362.4
Imperial Valley-06	1979	Compuertas	6.53	13.52	259.9
Northridge-01	1994	LA–116th St School	6.69	36.39	301.0
Northridge-01	1994	LA–N Figueroa St	6.69	30.19	364.9
Northridge-01	1994	LA–Temple & Hope	6.69	28.82	452.2
Northridge-01	1994	Manhattan Beach–Manhattan	6.69	33.56	351.6
Northridge-01	1994	Sunland–Mt Gleason Ave	6.69	12.38	402.2
Spitak, Armenia	1988	Gukasian	6.77	23.99	343.5
Chuetsu-oki	2007	Nadachiku Joetsu City	6.80	35.79	570.6
Kobe, Japan	1995	Abeno	6.90	24.85	256.0
Kobe, Japan	1995	Sakai	6.90	28.08	256.0
Iwate	2008	Yuzawa Town	6.90	22.41	655.5
Loma Prieta	1989	Fremont–Emerson Court	6.93	39.66	284.8
Darfield, New Zealand	2010	SBRC	7.00	21.31	263.2
El Mayor-Cucapah	2010	EJIDO SALTILLO	7.20	14.80	242.1
Landers	1992	Desert Hot Springs	7.28	21.78	359.0
Kern County	1952	Taft Lincoln School	7.36	38.42	385.4
Chi-Chi, Taiwan	1999	CHY046	7.62	24.10	442.2
Chi-Chi, Taiwan	1999	TCU060	7.62	8.51	375.4
Wenchuan, China	2008	Dayiyinping	7.90	28.59	378.9

B.3 Selected accelerograms for models BT2_SM and BT2_SM-BM at damage state D_3

Earthquake name	Year	Station name	Moment magnitude M_w (-)	Joyner-Boore distance (km)	$V_{S,30}$ (m/s)
Whittier Narrows-01	1987	Compton–Castlegate St	5.99	18.32	266.9
Whittier Narrows-01	1987	Downey–Birchdale	5.99	14.90	245.1
Parkfield-02, CA	2004	Parkfield–Fault Zone 3	6.00	1.10	211.7
Parkfield-02, CA	2004	PARKFIELD–UPSAR 07	6.00	9.14	440.6
Parkfield-02, CA	2004	PARKFIELD–UPSAR 11	6.00	8.93	466.1

Earthquake name	Year	Station name	Moment magnitude M_w (-)	Joyner-Boore distance (km)	$V_{S,30}$ (m/s)
Morgan Hill	1984	Anderson Dam (Downstream)	6.19	3.22	488.8
Kalamata, Greece-01	1986	Kalamata (bsmt)	6.20	6.45	382.2
Christchurch, New Zealand	2011	Christchurch Cashmere High School	6.2	4.44	204.0
Christchurch, New Zealand	2011	Riccarton High School	6.2	9.43	293.0
Christchurch, New Zealand	2011	Shirley Library	6.2	5.58	207.0
L'Aquila, Italy	2009	L'Aquila–V. Aterno -Colle Grilli	6.30	0.00	685.0
Victoria, Mexico	1980	Cerro Prieto	6.33	13.80	471.5
Coalinga-01	1983	Pleasant Valley P.P.–bldg	6.36	7.69	257.4
Friuli, Italy-01	1976	Tolmezzo	6.50	14.97	505.2
Imperial Valley-06	1979	Delta	6.53	22.03	242.1
Superstition Hills-02	1987	El Centro Imp. Co. Cent	6.54	18.20	192.1
Superstition Hills-02	1987	Poe Road (temp)	6.54	11.16	316.6
New Zealand-02	1987	Matahina Dam	6.60	16.09	551.3
Niigata, Japan	2004	NIG023	6.63	25.33	654.8
Erzican, Turkey	1992	Erzincan	6.69	0.00	352.1
Northridge-01	1994	Arleta–Nordhoff Fire Sta	6.69	3.3	297.7
Northridge-01	1994	LA–Hollywood Stor FF	6.69	19.73	316.5
Northridge-01	1994	Los Angeles–7-story Univ Hospital (FF)	6.69	32.39	332.3
Northridge-01	1994	LA 00	6.69	9.87	706.2
Northridge-01	1994	Sun Valley–Roscoe Blvd	6.69	5.59	320.9
Chuetsu-oki	2007	Joetsu Yanagishima paddocks	6.80	28.07	605.7
Chuetsu-oki	2007	Yoshikawaku Joetsu City	6.80	13.68	561.6
Chuetsu-oki	2007	Kashiwazaki City Center	6.80	0.00	294.4
Chuetsu-oki	2007	Yoitamachi Yoita Nagaoka	6.80	4.69	655.5
Chuetsu-oki	2007	Kawanishi Izumozaki	6.80	0.00	338.3
Kobe, Japan	1995	Kakogawa	6.90	22.50	312.0
Loma Prieta	1989	Gilroy–Gavilan Coll	6.93	9.19	729.7
Loma Prieta	1989	Gilroy Array #4	6.93	13.81	221.8
Darfield, New Zealand	2010	Kaiapoi North School	7.00	30.53	255.0
Hector Mine	1999	Hector	7.13	10.35	726.0
El Mayor-Cucapah	2010	Calexico Fire Station	7.20	19.12	231.2
Tabas, Iran	1978	Dayhook	7.35	0.00	471.5
Chi-Chi, Taiwan	1999	TCU089	7.62	0.00	671.5
Wenchuan, China	2008	Jiangyouchonghua	7.90	27.23	430.5
Wenchuan, China	2008	Anxiantashui	7.90	0.00	376.1

B.4 Selected accelerograms for models BT2_SM and BT2_SM-BM at damage state D_4

Earthquake name	Year	Station name	Moment magnitude M_w (-)	Joyner-Boore distance (km)	$V_{S,30}$ (m/s)
Yountville	2000	Napa Fire Station #3	5.00	8.48	328.6
Mammoth Lakes-06	1980	Long Valley Dam (Upr L Abut)	5.94	9.65	537.2
Whittier Narrows-01	1987	Downey–Birchdale	5.99	14.90	245.1
Parkfield-02, CA	2004	Parkfield–Fault Zone 3	6.00	1.10	211.7
Parkfield-02, CA	2004	PARKFIELD–UPSAR 07	6.00	9.14	440.6
Parkfield-02, CA	2004	PARKFIELD–UPSAR 11	6.00	8.93	466.1
Parkfield	1966	Cholame–Shandon Array #5	6.19	9.58	289.6
Morgan Hill	1984	Anderson Dam (Downstream)	6.19	3.22	488.8
Christchurch, New Zealand	2011	Christchurch Botanical Gardens	6.20	5.52	187.0
Christchurch, New Zealand	2011	Christchurch Cashmere High School	6.20	4.44	204.0
Christchurch, New Zealand	2011	Riccarton High School	6.20	9.43	293.0
Christchurch, New Zealand	2011	Shirley Library	6.20	5.58	207.0
Managua, Nicaragua-01	1972	Managua, ESSO	6.24	3.51	288.8
L'Aquila, Italy	2009	L'Aquila–V. Aterno -Colle Grilli	6.30	0.00	685.0
Victoria, Mexico	1980	Cerro Prieto	6.33	13.80	471.5
Coalinga-01	1983	Pleasant Valley P.P.–bldg	6.36	7.69	257.4
Friuli, Italy-01	1976	Tolmezzo	6.50	14.97	505.2
Superstition Hills-02	1987	Poe Road (temp)	6.54	11.16	316.6
Niigata, Japan	2004	NIG023	6.63	25.33	654.8
Erzican, Turkey	1992	Erzincan	6.69	0.00	352.1
Northridge-01	1994	Canoga Park–Topanga Can	6.69	0.00	267.5
Northridge-01	1994	LA–Hollywood Stor FF	6.69	19.73	316.5
Northridge-01	1994	Los Angeles–7-story Univ Hospital (FF)	6.69	32.39	332.3
Northridge-01	1994	LA 00	6.69	9.87	706.2
Northridge-01	1994	Sun Valley–Roscoe Blvd	6.69	5.59	320.9
Chuetsu-oki	2007	Yoshikawaku Joetsu City	6.80	13.68	561.6
Chuetsu-oki	2007	Kashiwazaki City Center	6.80	0.00	294.4
Chuetsu-oki	2007	Yoitamachi Yoita Nagaoka	6.80	4.69	655.5
Chuetsu-oki	2007	Kawanishi Izumozaki	6.80	0.00	338.3
Chuetsu-oki	2007	NIG018	6.80	0.00	198.3
Loma Prieta	1989	Gilroy–Gavilan Coll	6.93	9.19	729.7
Darfield, New Zealand	2010	DFHS	7.00	11.86	344.0
Darfield, New Zealand	2010	Kaiapoi North School	7.00	30.53	255.0
El Mayor-Cucapah	2010	MICHOACAN DE OCAMPO	7.20	13.21	242.1
El Mayor-Cucapah	2010	El Centro–Imperial & Ross	7.20	19.39	229.3
Tabas, Iran	1978	Dayhook	7.35	0.00	471.5
Chi-Chi, Taiwan	1999	TCU067	7.62	0.62	433.6
Chi-Chi, Taiwan	1999	TCU089	7.62	0.00	671.5

Earthquake name	Year	Station name	Moment magnitude M_w (-)	Joyner-Boore distance (km)	$V_{S,30}$ (m/s)
Wenchuan, China	2008	Jiangyouchonghua	7.90	27.23	430.5
Wenchuan, China	2008	Anxiantashui	7.90	0.00	376.1

Acknowledgements The authors gratefully acknowledge the financial support of the PRIN-2017 project DETECT-AGING (Project code 201747Y73L) funded by the Italian Ministry of Education, University and Research, and the financial support of the Emilia-Romagna regional agency for Civil Protection and Territorial Safety.

Author contributions All authors contributed to the study conception and methodology. The funding acquisition was performed by Claudio Mazzotti and Nicola Buratti. Material preparation, data collection and analysis were performed by Francesca Ferretti and Elena Simoni. The first draft of the manuscript was written by Francesca Ferrett and Elena Simoni and all authors commented on previous versions of the manuscript. All authors read and approved the final manuscript.

Funding Open access funding provided by Alma Mater Studiorum - Università di Bologna within the CRUI-CARE Agreement. The present work received the financial support of the PRIN-2017 project DETECT-AGING (Project code 201747Y73L) funded by the Italian Ministry of Education, University and Research, and the financial support of the Emilia-Romagna regional agency for Civil Protection and Territorial Safety.

Data availability The datasets generated during and/or analysed during the current study are available from the corresponding author upon reasonable request.

Declarations

Conflict of interest The authors have no relevant financial or non-financial interests to disclose.

References

Applied Technology Council (1996) ATC 40 seismic evaluation and retrofit of concrete buildings Redwood City California. Seism Saf Commisionsion 1:334

Baggio C, Bernardini A, Colozza R et al (2002) Manuale per la compilazione della scheda di 1° livello di rilevamento del danno, pronto intervento e agibilità per edifici ordinari nell'emergenza post-sismica (AeDES), pp 1–119

Battaglia L, Ferreira TM, Lourenço PB (2021) Seismic fragility assessment of masonry building aggregates: a case study in the old city Centre of Seixal, Portugal. Earthq Eng Struct Dyn 50:1358–1377. https://doi.org/10.1002/eqe.3405

Boore DM, Watson-Lamprey J, Abrahamson NA (2006) Orientation-independent measures of ground motion. Bull Seismol Soc Am 96:1502–1511. https://doi.org/10.1785/0120050209

Box GEP, Draper NR (1987) Empirical Model-Building and Response Surfaces. John Wiley and Sons (Ed.)

Box GEP, Wilson KB (1951) On the experimental attainment of optimun conditions. J R Stat Soc 13:1–45

Bracchi S, Rota M, Penna A, Magenes G (2015) Consideration of modelling uncertainties in the seismic assessment of masonry buildings by equivalent-frame approach. Bull Earthq Eng 13:3423–3448. https://doi.org/10.1007/s10518-015-9760-z

Buratti N, Ferracuti B, Savoia M (2010) Response Surface with random factors for seismic fragility of reinforced concrete frames. Struct Saf 32:42–51. https://doi.org/10.1016/j.strusafe.2009.06.003

Calvi GM (1999) A displacement-based approach for vulnerability evaluation of classes of buildings. J Earthq Eng 3:411–438. https://doi.org/10.1080/13632469909350353

Cattari S, Angiolilli M (2022) Multiscale procedure to assign structural damage levels in masonry buildings from observed or numerically simulated seismic performance. Bull Earthq Eng 20:7561–7607. https://doi.org/10.1007/s10518-022-01504-x

Cattari S, Lagomarsino S, Ottonelli D (2014) Fragility curves for masonry buildings from empirical and analytical modelS. In: Second European Conference on Earthquake Engineering and Seismology. Istanbul, Turkey

Cattari S, Curti E, Giovinazzi S et al (2004) A model for vulnerabilty analysis of masonry building at urban scale (in Italian). In: XI Congresso Nazionale "L'Ingegneria Sismica in Italia" - ANIDIS

CEN (2004) Eurocode 8: Design of structures for earthquake resistance —

Ceroni F, Pecce M, Sica S, Garofano A (2012) Assessment of seismic vulnerability of a historical masonry building. Buildings 2:332–358. https://doi.org/10.3390/buildings2030332

CNR-DT212/2013 (2014) Istruzioni per la Valutazione Affidabilistica della Sicurezza Sismica di Edifici Esistenti (in Italian). Natl Res Counc, p 190

Fajfar P (1999) Capacity spectrum method based on inelastic demand spectra. Earthq Eng Struct Dyn 28:979–993. https://doi.org/10.1002/(SICI)1096-9845(199909)28:9%3c979::AID-EQE850%3e3.0.CO;2-1

Fajfar P (2000) A Nonlinear Analysis Method for Performance-Based Seismic Design. Earthq Spectra 16:573–592. https://doi.org/10.1193/1.1586128

Fajfar P, Fischinger M (1988) N2–A method for non-linear seismic analysis of regular buildings. In: Science Council of Japan (ed) Proceedings of the 9th World Conference on Earthquake Engineering. Tokyo, Japan, pp 111–116

Faravelli L (1989) Response-surface approach for reliability analysis. J Eng Mech 115:2763–2781. https://doi.org/10.1061/(ASCE)0733-9399(1989)115:12(2763)

FEMA (1999) Technical and user's manual of advanced engineering building module (AEBM) - earthquake loss estimation methodology hazus - MH 2.1

Ferretti F, Ferracuti B, Mazzotti C, Savoia M (2019) Destructive and minor destructive tests on masonry buildings: experimental results and comparison between shear failure criteria. Constr Build Mater 199:12–29. https://doi.org/10.1016/j.conbuildmat.2018.11.246

Ferretti F, Mazzotti C, Ferracuti B, Tilocca AR (2016) Mohr-Coulomb failure domain of rural masonry through slightly-destructive tests. In: Proceedings of the 10th Structural Analysis of Historical Constructions SAHC: Anamnesis, Diagnosis, Therapy Control, pp 1316–1323

Franchin P, Lupoi A, Pinto PE, Schotanus MI (2003) Seismic fragility of reinforced concrete structures using a response surface approach. J Earthq Eng 7:45–77. https://doi.org/10.1080/13632460309350473

Freeman SA (1994) The capacity spectrum method for determining the demand displacement. In: ACI 1994 spring convention

Freeman SA (2004) Review of the development of the capacity spectrum method. ISET J Earthq Technol 41:113

Guerrini G, Graziotti F, Penna A, Magenes G (2017) Improved evaluation of inelastic displacement demands for short-period masonry structures. Earthq Eng Struct Dyn 46:1411–1430. https://doi.org/10.1002/eqe.2862

Indirli M, Kouris SLA, Formisano A et al (2013) Seismic damage assessment of unreinforced masonry structures after the Abruzzo 2009 earthquake: the case study of the historical centers of L'Aquila and Castelvecchio Subequo. Int J Archit Herit 7:536–578. https://doi.org/10.1080/15583058.2011.654050

Ioannou I, Bertelli S, Verrucci E et al (2021) Empirical fragility assessment of residential buildings using data from the Emilia 2012 sequence of earthquakes. Springer, Netherlands

Jacobsen LS (1930) Steady forced vibrations as influenced by damping. In: ASME (ed) Transactions of the American Society of Mechanical Engineers, pp 169–181

Jaiswal K, Wald D, D'Ayala DF (2011) Developing empirical collapse fragility functions for global building types. Earthq Spectra 27:775–795. https://doi.org/10.1193/1.3606398

Khuri AI, Cornell JA (1997) Response surfaces: design and analyses. New York City

Lagomarsino S, Cattari S (2014) Fragility functions of masonry buildings. In: Pitilakis K, Crowley H, Kaynia A (eds) SYNER-G: Typology Definition and Fragility Functions for Physical Elements at Seismic

Risk. Geotechnical, Geological and Earthquake Engineering, vol 27. Springer, Dordrecht. https://doi.org/10.1007/978-94-007-7872-6_5
Lagomarsino S, Cattari S (2015) PERPETUATE guidelines for seismic performance-based assessment of cultural heritage masonry structures. Bull Earthq Eng 13:13–47. https://doi.org/10.1007/s10518-014-9674-1
Lagomarsino S, Giovinazzi S (2006) Macroseismic and mechanical models for the vulnerability and damage assessment of current buildings. Bull Earthq Eng 4:415–443. https://doi.org/10.1007/s10518-006-9024-z
Lagomarsino S, Penna A, Galasco A, Cattari S (2013) TREMURI program: an equivalent frame model for the nonlinear seismic analysis of masonry buildings. Eng Struct 56:1787–1799. https://doi.org/10.1016/j.engstruct.2013.08.002
Lourenço PB, Mendes N, Ramos LF, Oliveira DV (2011) Analysis of masonry structures without box behavior. Int J Archit Herit 5:369–382. https://doi.org/10.1080/15583058.2010.528824
Mann W, Muller H (1980) Failure of shear-stressed masonry: an enlarged theory, tests and application to shear walls. In: Proceedings of the International Syposium on Load Bearing Brickwork, London
Milani G, Benasciutti D (2010) Homogenized limit analysis of masonry structures with random input properties: polynomial response surface approximation and Monte Carlo simulations. Struct Eng Mech 34:417–447. https://doi.org/10.12989/sem.2010.34.4.417
Milosevic J, Cattari S, Bento R (2020) Definition of fragility curves through nonlinear static analyses: procedure and application to a mixed masonry-RC building stock. Bull Earthq Eng 18:513–545. https://doi.org/10.1007/s10518-019-00694-1
Ministero delle Infrastrutture e dei Trasporti (2018) Aggiornamento delle «Norme tecniche per le costruzioni» (in Italian). Gazz Uff della Repubb Ital
Ministero delle Infrastrutture e dei Trasporti (2019) Istruzioni per l'applicazione dell'«Aggiornamento delle "Norme tecniche per le costruzioni"» di cui al decreto ministeriale 17 gennaio 2018. Gazz Uff della Repubb Ital
Pacific Earthquake Engineering Research Center PEER Ground Motion Database. https://ngawest2.berkeley.edu/
Parisi F, Augenti N (2012) Uncertainty in seismic capacity of masonry buildings. Buildings 2:218–230. https://doi.org/10.3390/buildings2030218
Parisi F, Augenti N (2013) Earthquake damages to cultural heritage constructions and simplified assessment of artworks. Eng Fail Anal 34:735–760. https://doi.org/10.1016/j.engfailanal.2013.01.005
Penna A, Lagomarsino S, Galasco A (2014a) A nonlinear macroelement model for the seismic analysis of masonry buildings. Earthq Eng Struct Dyn 43:159–179. https://doi.org/10.1002/eqe.2335
Penna A, Morandi P, Rota M et al (2014b) Performance of masonry buildings during the Emilia 2012 earthquake. Bull Earthq Eng 12:2255–2273. https://doi.org/10.1007/s10518-013-9496-6
Rajashekhar MR, Ellingwood BR (1993) A new look at the response surface approach for reliability analysis. Struct Saf 12:205–220. https://doi.org/10.1016/0167-4730(93)90003-J
Rota M, Penna A, Strobbia CL (2008) Processing Italian damage data to derive typological fragility curves. Soil Dyn Earthq Eng 28:933–947. https://doi.org/10.1016/j.soildyn.2007.10.010
Rota M, Penna A, Magenes G (2014) A framework for the seismic assessment of existing masonry buildings accounting for different sources of uncertainty. Earthq Eng Struct Dyn 43:1045–1066. https://doi.org/10.1002/eqe.2386
Shinozuka M, Feng MQ, Lee J, Naganuma T (2000) Statistical analysis of fragility curves. J Eng Mech 126:1224–1231
Silva V, Crowley H, Varum H et al (2014) Evaluation of analytical methodologies used to derive vulnerability functions. Earthq Eng Struct Dyn 43:181–204. https://doi.org/10.1002/eqe.2337
Simões A, Milošević J, Meireles H et al (2015) Fragility curves for old masonry building types in Lisbon. Bull Earthq Eng 13:3083–3105. https://doi.org/10.1007/s10518-015-9750-1
Sousa L, Silva V, Marques M, Crowley H (2016) On the treatment of uncertainties in the development of fragility functions for earthquake loss estimation of building portfolios. Earthq Eng Struct Dyn 45:1955–1976. https://doi.org/10.1002/eqe.2734
Turnsek V, Cacovic F (1971) Some experimental results on the strength of brick masonry walls. In: Proceedings of the 2nd international brick masonry conference. Stoke-on-Trent, United Kingdom
Vidic T, Fajfar P, Fischinger M (1994) Consistent inelastic design spectra: strength and displacement. Earthq Eng Struct Dyn 23:507–521. https://doi.org/10.1002/eqe.4290230504